ACS APPLIED MATERIALS & INTERFACES

www.acsami.org

Research Article

Transient Interfacial Pattern Formation in Block Copolymer Thin Films via Sequential Thermal and Solvent Immersion Annealing

Kshitij Sharma, Maninderjeet Singh, Sushil K. Satija, John F. Ankner, Jack F. Douglas,* and Alamgir Karim*

Cite This: *ACS Appl. Mater. Interfaces* 2024, 16, 15569−15585

Read Online

ACCESS | Metrics & More | Article Recommendations | Supporting Information

ABSTRACT: A variety of structures encountered in nature only arise in materials under highly nonequilibrium conditions, suggesting to us that the scope for creating new functional block copolymer (BCP) structures might be significantly enlarged by embracing complex processing histories that allow for the fabrication of structures quite unlike those created under "near-equilibrium" conditions. The present work examines the creation of polymer film structures in which highly nonequilibrium processing conditions allow for the creation of entirely new types of transient BCP morphologies achieved by transitioning between different ordered states. Most previous studies of BCP materials have emphasized ordering them from their disordered state obtained from a solution film casting process, followed by a slow thermal annealing (TA) process at elevated temperatures normally well above room temperature. We have previously shown that achieving the equilibrium TA state can be accelerated by a direct solvent immersion annealing (DIA) preordering step that creates nascent ordered microstructures, followed by TA. In the present work, we examine the reverse nonequilibrium sequential processing in which we first thermally anneal the BCP film to different levels of partial (lamellar) order and then subject it to DIA to swell the lamellae. This sequential processing rapidly leads to a swelling-induced wrinkle pattern that initially grows with immersion time and can be quenched by solvent evaporation into its corresponding glassy state morphology. The article demonstrates the formation of wrinkling "defect" patterns in entangled BCP films by this sequential annealing that does not form under ordinary TA conditions. At long DIA times, these highly "defective" film structures evolve in favor of the equilibrium morphology of parallel lamellae observed with DIA alone. In conjunction with our previous study of sequential DIA + TA, the present TA + DIA study demonstrates that switching the order of these processing methods for block copolymer films gives the same final state morphology in the limit of long time as any one method alone, but with drastically different intermediate transient state morphologies. These transient morphologies could have many applications.

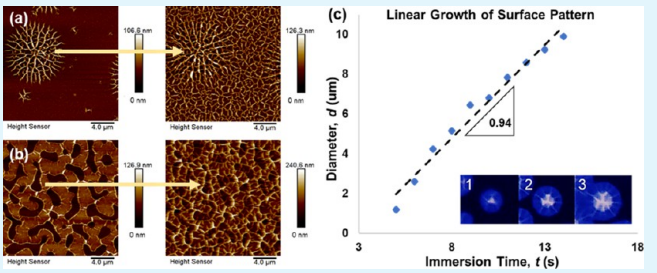

KEYWORDS: *block copolymers, order−order transition, thin films, thermal annealing, direct immersion annealing, nonequilibrium, wrinkling, neutron reflectivity*

INTRODUCTION

As a way of general background, block copolymers (BCPs) are macromolecules composed of chemically distinct blocks that microphase separate into a wide range of equilibrium morphologies with scientific and industrial importance. These ordered structures range from body-centered cubic spheres for highly asymmetric volume fractions to hexagonally packed cylinders followed by flat layers or lamellae for more symmetric volume fractions.[1] A myriad of applications take advantage of these self-assembled microstructures, including membranes,[2,3] plasmonic devices,[4−6] high-density memory storage devices,[7] nanolithography templates,[8] and dielectric devices.[9,10] Most of these applications require a high level of control of multiple microstructural parameters, which depend heavily on the processing methodology used to produce these ordered structures. Hence, fabricating these structures is often more of an art than a science.

The thermodynamics of block copolymer (BCP) equilibrium microphase separation is governed by a few primary molecular parameters whose variation enables some control on nonequilibrium BCP film morphologies. These molecular parameters include the degree of polymerization (N) and a phenomenological Flory−Huggins interaction parameter (χ). A single parameter, the product χN, is often taken as the measure of the thermodynamic driving force toward microphase ordering. In this model, increasing N enhances the segregation between the polymer components of BCP and

Received: January 2, 2024
Revised: February 28, 2024
Accepted: February 28, 2024
Published: March 14, 2024

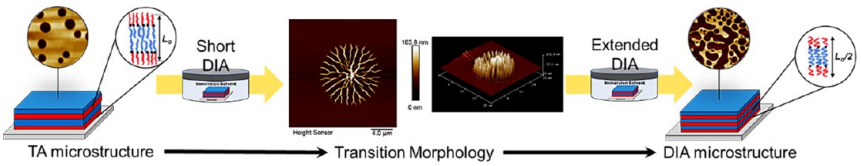

Figure 1. Sequential annealing method of TA followed by DIA. The lamellar BCP film exhibits a transient wrinkle patterned surface when exposed to the solvent, which we discuss in detail below.

causes the chains in the segregated polymer domains of the BCP to swell. Increasing the chain length at fixed T inevitably leads to a sharp slowing down of polymer dynamics due to chain entanglement, so the increase in interaction strength between the polymer blocks χN that can be achieved by increasing N alone is practically limited. Sequential annealing methods have recently gained popularity in recent efforts to overcome these kinetic limitations. This approach is desirable for synthesizing new materials where novel structures emerge under far-from-equilibrium processing conditions. It is also possible to address kinetic bottlenecks through this type of method. For example, we previously reported that the rapid ordering of lamellae in BCP films could be obtained from an initial ordering of the material by immersion in a mixed solvent (termed direct immersion annealing, DIA) for a short time that traps a metastable morphology, followed by a period of conventional thermal annealing, TA, i.e., DIA + TA to achieve equilibrium.[11] In this article, our interest is in the reverse annealing process of TA + DIA. To understand this sequential process better, we briefly review DIA for the readers unfamiliar with the methodology.

Previously, we have shown that direct immersion annealing (DIA) of as-cast polymer film leads to accelerated ordering.[12] In this method, the immersion solvent mixture is primarily composed of a nonsolvent, so that the complete dissolution of the film is prevented or greatly inhibited, and after a short time, the presence of an additional good-neutral solvent for the polymer blocks can cause the entire BCP film to swell and order rapidly. Having the good solvent be selective to one of the blocks of the BCP also increases the effective value of χ, giving rise to a greatly enhanced thermodynamic driving force for BCP film ordering.[13] DIA clearly involves ordering the BCP films under far from equilibrium conditions, so this processing method corresponds to a significant departure from TA and enhanced TA processing.

Modi et al. and Longanecker et al. have studied DIA for both asymmetric and symmetric diblock copolymer systems and demonstrated that it induces rapid BCP ordering.[12,13] Due to the solvent environment being static (sealed solvent bath) in their studies, swelling conditions are solely governed by the polymer−solvent interactions where the solvent composition is easy to control. Also, chemical potentials are higher inside the relatively dense solvent than in its vapor environment, which may lead to greater film swelling. Besides the methods mentioned above, several other novel approaches are being studied, including microwave annealing,[14] solvothermal annealing,[15] laser field annealing,[16] and electric/magnetic field induced annealing.[17,18]

Strikingly, DIA has been shown to produce ordered microdomains in processing times of minutes rather than hours required for typical TA processing. Moreover, this type of solvent annealing can be performed at room temperature, so it is applicable to polymers that become thermally unstable at the relatively high temperature required for TA processing. Besides the fast processing kinetics of this technique, ordered BCP films having a parallel lamellar morphology are formed due to the preferential segregation of one block to the substrate or air interface. DIA produces domains with reduced size and smaller interfacial width. Longanecker et al. reported up to ≈50% reduction in parallel lamellar domain size (compared to TA; $L_{o,DIA} \approx 0.5\ L_{o,TA}$) for a poly(styrene-*b*-methyl methacrylate) (Number-average molecular mass, M_n = 36.5 kg/mol) thin film upon DIA in a solvent mixture composed of heptane, acetone, and toluene.[13] The reduction in solvent-processed BCP domain sizes is due to the trapping of large junction spacing of the solvent-swollen lamellar structure by quick solvent evaporation. The trapped chains take up a collapsed conformation producing thinner layers, compared to stretched chains of the TA microstructure. Figure S1 describes this disparity. The modification in BCP segmental interaction (χ parameter) due to solvent selectivity and its preferential segregation normally causes a reduction in the interfacial widths.[19] The BCP χ in the DIA solvent mixture can be manipulated—it can be lower due to the presence of a neutral good solvent (toluene), or, in the presence of a significant quantity of a block (poly(methyl methacrylate)) selective solvent like acetone, χ is higher than that in the melt. Regardless, with solvent evaporation, thinner domains evolve in the solvent-processed films and develop into parallel lamellar domains with significantly reduced domain size (as much as 50% reduction) compared to those in the melt-processed TA microstructure. The DIA lamellar morphology, therefore, has a higher contact area between dissimilar polymers (polystyrene and poly(methyl methacrylate) or PS and PMMA, respectively) due to the increased number of interfaces, giving a microstructure with higher interfacial energy and a metastable position on a free energy diagram.

In a previous publication, we reported this energy disparity between the different lamellar microstructures for the same BCP.[11] We showed that these energy states for a BCP can be cascaded via process design to develop combinatorial processing strategies to hike down the free energy landscape in steps for facile self-assembly. We also demonstrated that a multi terraced island-hole transition morphology could be produced using the sequential methodology, which is not achievable by other techniques. Combinatorial BCP processing methods have been reported before, especially parallel solvent vapor annealing (SVA) + thermal annealing or the solvothermal annealing method.[15,20] Other approaches include parallel SVA + microwave annealing and a sequential SVA to TA process.[14,21] The solvothermal annealing procedure accelerated BCP self-assembly via enhanced swelling due to the increased vapor pressure at a higher temperature, and the sequential annealing study was focused on directed self-assembly (DSA) with little emphasis on the kinetics of the process. These studies achieved targeted morphologies but did not account for interesting transition states that may be facilitating the assembly.

https://doi.org/10.1021/acsami.4c00068
ACS Appl. Mater. Interfaces 2024, 16, 15569−15585

The transformation pathway for any system changing from a high to a low free energy state requires "activation energy" to overcome thermodynamic barriers in a reasonable time scale. In contrast, driving a system from a low energy (TA microstructure), as in the BCP polymer system that we study here, to a high energy (DIA) microstructure is expected to require much higher thermal activation energies and processing times. In this article, we focus on establishing such nonequilibrium conditions through a simple sequential annealing process and study the BCP morphology evolution from a disordered as-cast state to a free energy minimum state by TA and finally to a metastable state by DIA through a high surface area transition morphology as shown in Figure 1. In essence, we order the films first using TA, followed by two different solvent annealing methods, a mixed vapor phase contact process, and a direct contact of the BCP film with a judiciously chosen solvent mixture, i.e., liquid phase contact. Tracking these sequential transitions provides information on developing pathways to obtain unique metastable and transition structures from equilibrium ones, i.e., a controlled hike up the energy landscape. We also find that the surface roughness and surface pattern evolution of the BCP films can be controlled through the choice of the time of the first TA step and by controlling the solvent environment of the second DIA immersion step.

Surface patterns have been reported for solvent swelling of surface cross-linked polymer films and very thin metal films on soft substrates[22−24] that are formed by buckling at the interface due to a differential expansion of parallel layers on solvent absorption. The dimensions of these surface wrinkles in and out of the plane of the film can be used to derive the mechanical properties of these films. For instance, Chung et al. reported a direct relation between the wrinkling wavelength and the ratio of moduli between layers.[24] We see a clear manifestation of this in the scale of the PS-*b*-PMMA wrinkle pattern (nm), compared to those observed by Chung and co-workers (μm). This is due to a much smaller modulus mismatch between the TA-ordered PS and PMMA layers. With further annealing, this wrinkling instability grows through the entire film, both in lateral and perpendicular directions, and destabilizes it, producing a highly rough film surface. The degree of film surface disruption and evolution kinetics were studied for a series of BCP molecular masses above and below the entanglement molecular masses (dilution conditions). In addition to DIA as a second processing step, we studied SVA as the second processing step post-TA. The swelling potentials in SVA are lower than DIA but still higher than those observed for a melt during TA alone. The degree of surface pattern formation produced by sequential SVA was, therefore, observed to be lower than that produced by sequential DIA. An interesting aspect of this sequential processing methodology is that the wrinkling structures are transient, and the BCP film ultimately "heals" back to the regular DIA/SVA lamellar morphology with a reduced domain size ($L_{o,DIA}$/$L_{o,SVA}$).

The microstructure evolution is tracked through atomic force microscopy (AFM) imaging to quantify the surface topography of the parallel lamellar microstructure. To probe the internal order of the films, Neutron Reflectivity (NR) is employed to obtain the degree and dimensions of the lamellar domain inside the film using partially deuterated BCPs. Sequential annealing for intermediate TA and DIA is also reported to elaborate upon the role of the degree of pre-TA order on the secondary DIA treatment and to optimize the methodology. The transitions have been described schematically with an energy diagram to reiterate the energetics and processing kinetics between the transitioning morphologies. When processed using this sequential pathway, the BCP material is inherently in a non-equilibrium state, but the intermediate structures seem suitable for new applications. This is the normal situation in living systems where dissipative structures are formed under nonequilibrium conditions. We embrace the possibilities that this method of fabrication opens for us.

RESULTS AND DISCUSSION

Morphology Variation in Direct Immersion Annealed (DIA) versus Thermally Annealed (TA) Films. Block copolymers offer a variety of microstructures that are not only dependent on their molecular architecture but also on the processing environment. Based on their morphology, there can be a myriad of applications. While TA and DIA produce parallel lamellar morphology for symmetric PS-*b*-PMMA on SiO_x substrates owing to the segregation of PMMA to SiO_x,[25−27] SVA can neutralize interactions with the substrate and produce a vertical orientation.[28,29] TA (equilibrium) and DIA (stable under DIA conditions, but metastable relative to TA) morphologies, although both are parallel with regards to the orientation of the lamellae relative to the film surface, differ in domain size, interfacial width, and number of unlike interfaces and, therefore, have intrinsically different interfacial energy. This gives us reference states to compare the two microstructures and track structural evolution between these states. For the DIA to TA sequential process reported in a previous publication,[11] the reduction in interfacial energy and the availability of multiple ordering fronts along with large junction spacings at the initial DIA ordered interfaces enhances the kinetics of the reassembly process from DIA to TA morphology. The use of short sequential TA treatments to relieve stress from the collapsed chain structure of the rapidly ordered DIA morphology showed how sequential annealing can synergistically affect microstructure development while enhancing assembly kinetics. In the current work, we aim to explore and understand film ordering kinetics, morphology evolution, chain diffusion mechanisms, and energetics of transition from both equilibrium (long-time TA) and non-equilibrium (short-time TA) ordered BCPs to unique metastable (short and intermediate time DIA or SVA) microstructure development which is the focus of the paper, and finally to equilibrium microstructures (long-time DIA or SVA). [We recap to readers that Masud et al. showed that one domain spacing ($1L_o$) high islands and holes develop, when the film internal lamellar structures are fully ordered as measured by NR, but partial internal ordering produced surface island-hole features with fractional L_o size].[30] We accomplish this using thin PS-*b*-PMMA films cast on SiO_x substrates (Ultraviolet Ozone (UVO) treated to develop a SiO_x layer) with different as-cast thicknesses in the range of 120−180 nm for different BCP molecular masses and subjecting them to differential swelling environments. Variable film thicknesses ensure more than one lamellar layer in the films (4 to 6 lamellar domains), and higher thicknesses are primarily used for films of high M_n BCPs with thicker lamellar domains. The films were annealed via the sequential treatment: (1) Long or short time TA of the as-cast film followed by (2) DIA of the TA-ordered film. The TA films develop island-hole

https://doi.org/10.1021/acsami.4c00068
ACS Appl. Mater. Interfaces 2024, 16, 15569−15585

topography, indicating the formation of parallel lamellar morphology in the film interior and that the film thicknesses used were incommensurate with the lamellar periods.[31,32] Their topography is characterized using atomic force microscopy (AFM).

Longanecker et al. studied lamellar dPS-*b*-PMMA (19.5k-*b*-18.1k) films via NR to obtain domain sizes, L_o of 25.9 nm for TA ($L_{o,TA}$), and 14.7 nm for DIA-processed ($L_{o,DIA}$) films.[13] The height of the island-hole features for the incommensurate film thickness corresponded to the equilibrium domain size ($1L_o$) of the BCP for the particular treatment method.[30,33,34] We performed AFM height sensor scans and used the average island-hole heights to estimate equilibrium long-time annealed domain sizes listed in Table 1. These control measurements provided the domain spacing obtained after processing separately with TA and DIA from a disordered as-cast state. They will be used as comparative end point morphologies between TA- and DIA-induced structural transitions.

Table 1. Polystyrene-*b*-poly(methyl methacrylate) Block Copolymer Molecular Masses and Average Experimental Microstructure Dimensions[a]

PS-*b*-PMMA M_n (kg/mol)	thermal $L_{o,TA}$ (nm)	DIA $L_{o,DIA}$ (nm)
36.5 (19-*b*-17.5)	21	14
51 (25-*b*-26)	28	20
66 (33-*b*-33)	35	27
89 (45-*b*-44)	45	33
62 (32.5-*b*-29.5)	36	25

[a]dPS-*b*-PMMA used in NR studies.

The time needed for thermal annealing to achieve equilibrium microstructure ranged from 24 h for M_n = 36.5 to 66 k at 180 °C to 48 h for M_n = 89 k at 200 °C. The order−disorder temperatures (T_{ODT}) for this BCP were reported by Ahn et al. for M_n = 29.2 k and M_n = 35.6 k to be 200 and 250 °C, respectively, and they showed that the T_{ODT} increased with increasing molecular mass.[35] To achieve the metastable DIA microstructure from an as-cast film, the DIA treatment time ranged from 1 h for M_n = 27 to 66 k in SM_1 (solvent mixture 1 ≈ 75% heptane, 20% acetone, and 5% toluene by volume; details in the Experimental Section) to 3 h for M_n = 89 k in SM_2. DIA for BCP with M_n = 89 k in SM_1 was slower (up to 12 h) due to the lower diffusivity of high N chains, so a solvent mixture with a higher solubility parameter (SM_2 ≈ 60% heptane, 30% acetone, and 10% toluene by volume fraction−details in experimental methods) was necessary to achieve a higher degree of swelling and faster self-assembly. The domain sizes were much larger for TA ($L_{o,TA}$) than those produced by long-time equilibrium DIA (e.g., $L_{o,DIA} \approx 0.5\ L_{o,TA}$), a trend that is consistent with our previously published DIA studies. The difference is less prominent with increasing molecular mass and is due to differences in the degree of swelling with increasing entanglement. In the following study, the dynamics of the TA followed by a DIA sequential treatment are explored and explained based on the ease of chain diffusion (entanglements), change in interfacial energies, and disruptions caused by instantaneous wrinkling of the TA lamellar microstructure on immersion in a DIA solvent mixture.

Sequential TA + DIA Annealing-Induced Surface Pattern and Morphological Transitions. Lamellae forming *sym* PS-*b*-PMMA with total molecular mass ranging from 36.5 to 89 k (g/mol) were cast into thin films. Long-time thermal annealing (TA) for 24−48 h in vacuum produced a well-developed island-hole surface morphology indicative of a fully developed parallel lamellar structure, such that the island-hole height reflected the $1L_o$ BCP domain size, which increased with an increase in molecular mass of the BCP. These thermally annealed films were then successively annealed via DIA in solvent mixture SM_1 for molecular mass ranging from 36.5 to 66 k, and in SM_2 for films of molecular mass of 89 k. Annealing durations were selected for different molecular mass BCPs from conventional treatment times (30−90 min for M_n = 36.5 to 66k, and 3 h for M_n = 89k) required to achieve equilibrium morphology from a disordered as-cast state.[12,13] The island-hole film surface topography was tracked via AFM after each annealing step and is presented in Figure 2. The TA-processed films show a single-layered island-hole topography on the film surface with $L_{o,TA}$ domain size indicating a stable near-equilibrium structure. AFM characterization revealed that sequential annealing for conventional DIA times had a dramatically different effect on ordered films for BCPs with different M_n. For conventional DIA time, lower molecular mass (36.5 and 51 k, Figure 2-Row 3) films displayed complete order-to-order transition (OOT) into lamellar morphology with smaller DIA domain sizes ($L_{o,DIA}$). However, the island-hole topography was multilayered and required longer annealing times to produce the regular equilibrium single layer of island-hole.

In contrast, we observe a wrinkling pattern formation for higher M_n films, providing an interesting example of far-from-equilibrium pattern formation that would not be observed under near-equilibrium processing conditions. We found that BCP materials having a higher molecular mass (e.g., 66 and 89 k, Figure 2-Row 2), and thus a high degree of entanglement, give rise to a rather distinct morphology characterized by a highly undulating surface with surface features having a height that can even exceed the original film thickness. We attribute this morphology to the diffusive intrusion of the solvent into the PS and PMMA lamellar layers, and the resulting wrinkling of the film is caused by stresses produced during local swelling of the film.

This type of wrinkling pattern formation has been studied extensively in thin polymer film subjected to solvent intrusion at defects in the film surface.[24,36−38] We show some examples of these starburst type wrinkling patterns in Figure 3, which superficially resemble the growth and form of far-from-equilibrium polymer crystallization patterns in thin polymer films.[39] More irregular ("fractal") surface pattern formation have also been observed in BCP films subjected to stresses associated with large temperature changes.[40]

Figure 1 shows a schematic description of the sequential process of immersing a TA-ordered ($L_{o,TA}$) film in a solvent mixture to produce the undulating surface morphology and for the extended DIA treatment to produce the lamellar structure with reduced domain size ($L_{o,DIA}$). Optical images along with real space AFM height sensor images for the thermally annealed island-hole morphology for PS-*b*-PMMA (M_n = 66 k) and the subsequent dried transition morphology after short-time DIA immersion in SM_1 are shown in Figure S2 of the SI. The scans show a rapidly induced wrinkling instability after sequential DIA with the original TA island-hole boundaries still intact. Previous observations of the starburst-like wrinkling pattern formation found in Figure 3 were made in photo-cross-linked polymer films, which is natural because the instability requires the film to be an elastic material, and to have surface

https://doi.org/10.1021/acsami.4c00068
ACS Appl. Mater. Interfaces 2024, 16, 15569−15585

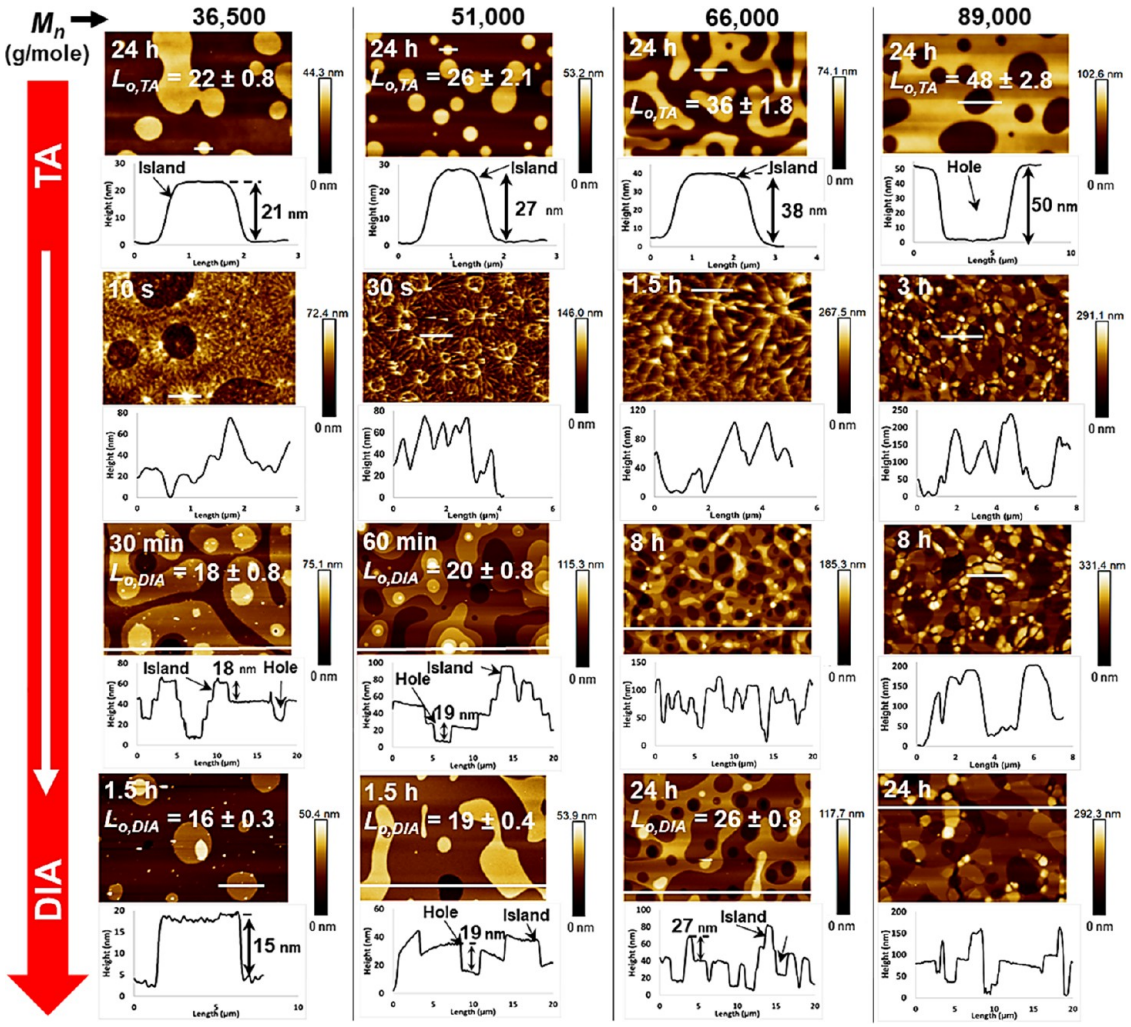

Figure 2. AFM height sensor images and line profiles showing topographical data. Row 1: *sym* PS-*b*-PMMA films annealed thermally at 180 °C (column 1−3: M_n = 36.5, 66, and 51 k) and 200 °C (column 4: M_n = 89 k) for 24 h showing well-developed island-hole morphology; Row 2: Rough transition morphologies with subsequent DIA treatments in SM_1 for M_n = 36.5, 51, 66 k and SM_2 for M_n = 89 k on pre-thermally annealed films for short time durations (inset); Row 3: Multilayered lamellar morphology with continued DIA treatment of prethermally annealed films; Row 4: BCP films for M_n = 36.5 and 51 k attaining complete transition to the DIA equilibrium domain size within 1.5 h of DIA treatment, while multilayered structure persists for BCP films of M_n = 66 and 89 k after 24 h of successive DIA treatment. Annealing times are in the images' top left, and numerical values in the line profile across marked lines in the images are approximate island-hole dimensions obtained via AFM in nm. L_o values are average island-hole heights in nm obtained from the images, and the uncertainty estimates are one standard deviation.

defects where the solvent intrudes into the film.[41] In our BCP film, the elasticity of the film material apparently derives from chain entanglement, and the kinetic hurdles in pattern formation are not observed in unentangled BCP films. We provide a preliminary study of the kinetics of wrinkling pattern growth below, following the methods of former studies of nonequilibrium crystal growth.[42]

We estimate the diameter of the "starburst-like" wrinkling patterns from in situ optical microscopy images by enclosing these patterns in a circle that just inscribes these structures for a range of DIA immersion times, and the results of this analysis are shown in Figure S3. The growth of the size of these wrinkling patterns is nearly linear in time (see Figure S3), with some slow oscillations about this growth, as observed previously in our polymer crystal growth in thin polymer films.[42,43] The measurement was initiated 5 s after film immersion, after which the wrinkle patterns could be readily discerned by optical microscopy.

The average rate of growth was found to be (1.02 ± 0.08) μm/s. Star-burst type swelling-induced wrinkling patterns arise from solvent intrusion into "defects" in the film's surface where the solvent is first "injected" into the film[24,41] (We quantify the topography of these patterns in Supporting Information). The linear growth of the wrinkling patterns suggests that the pattern formation can be described as an autocatalytic process.[44] We plan to provide detailed quantification of this wrinkling pattern formation in a separate publication devoted to this topic. This pattern formation process provides a good example of the potential of creating entirely new BCP structures by processing under far-from-equilibrium conditions. From a practical standpoint, we note that it should be possible to "lock in" this type of pattern using photo-cross-linking or some other chemical cross-linking method to create static structures useful in applications. We next consider the processing conditions leading to this beautiful variety of thin film pattern formation.

https://doi.org/10.1021/acsami.4c00068
ACS Appl. Mater. Interfaces 2024, 16, 15569−15585

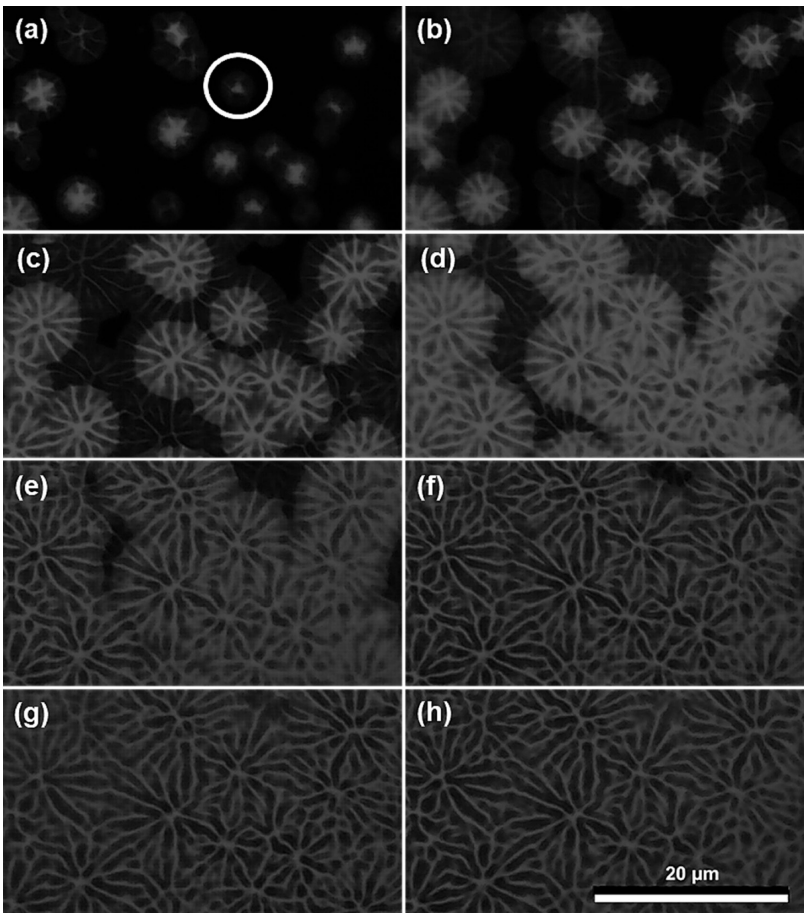

Figure 3. Snapshot images from an in situ optical microscopy Video S1 for the development of starburst-like wrinkling instability for a TA-ordered PS-*b*-PMMA (M_n = 66 k) film on sequential DIA in SM_1 for successive times after solvent exposure of (a) 7 s, (b) 10 s, (c) 12 s, (d) 15 s, (e) 18 s, (f) 20 s, (g) 23 s, and (h) 25 s.

Thermally annealed entangled BCP films with M_n = 66 and 89 k were sequentially annealed for extended DIA durations, and the films eventually produced a lamellar structure with a regular island-hole topography and reduced domain sizes. Before reaching a single surface layer of island-hole the films went through a multi-layered island-hole structure formation process with terraces of height $1L_{o,TA}$. This is shown for films with M_n = 36.5 to 66 k in Figure 2, Row 3, and for M_n = 89 k in Figure 2, Row 4. We observe that the scale of the multilayered pattern in the plane of the film decreases with an increase in the molecular mass of the films for similar annealing durations. This observation was also made by Smith et al. for the lateral growth of a single layer of island-hole pattern formed in lamellar PS-*b*-PMMA films.[32] The decrease in scale with increasing M_n is attributed to the increase in surface elasticity, i.e., an increase in the energetic cost of pattern formation. Contrastingly, the pattern growth rate for high-temperature thermal annealing displayed a first-order power law relation with annealing duration,[45] compared to the linear growth of the wrinkle pattern formed by immersion in solvent. The time scales of growth are, however, very different: hours for thermal annealing compared to seconds or minutes for solvent immersion annealing (DIA).

The wrinkled surface morphology produced by short-time DIA of a thermally ordered parallel lamellar microstructure is thus transient in nature. In the limit of long-time DIA, the film reorders into lamellar ordered states, similar to those formed after DIA ($L_{o,DIA}$) of an as-cast (disordered) film. The required successive DIA treatment durations to induce an order−order transition (OOT) from equilibrium TA to metastable DIA structures were, however, significantly higher for the high M_n BCPs, even though the molecular mass difference was not very high on shifting from M_n = 51 k to M_n = 66 k. The chain diffusion dynamics for these order-to-order transitions (OOTs) slowed down significantly with a small increase in M_n at this threshold. We hypothesize this is due to the nonlinear increase of the polymer solution viscosity with M_n and the BCP concentration because of chain entanglement. Thermally annealed films with M_n = 36.5 and 51 k were annealed for very short (<1 min) DIA treatments in SM_1 to test the universality of the transition morphology observed. A similar transition morphology with large undulating wrinkles was observed for the entire series of molecular masses tested, confirming the universal nature of wrinkling instability. The areal density of these features was found to be more concentrated near the island-hole boundaries for the very short (<1 min) sequential DIA treatment, and the wrinkles have a "wave-like" form for originally island-hole TA topography.

An estimation of the root-mean-square (RMS) roughness of the transient morphology with AFM height sensor imaging was made on an arbitrarily chosen area for a TA annealed sample, but where the region was free of any island-hole topography due to having a commensurate film thickness. The measure-

https://doi.org/10.1021/acsami.4c00068
ACS Appl. Mater. Interfaces 2024, 16, 15569−15585

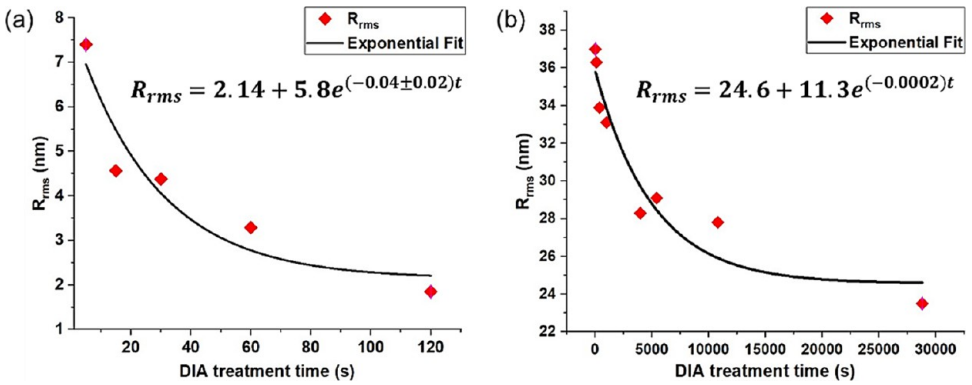

Figure 4. Root mean square roughness calculated for an AFM scan area of 400 μm^2 for a sample of PS-*b*-PMMA films annealed successively via DIA in SM_1 after a thermal annealing treatment at 180 °C for 24 h, (a) M_n= 25k-*b*-26k, and (b) M_n = 33k-*b*-33k.

ments were performed at different times of the sequential DIA, starting from the TA annealed state (at 180 °C for 24 h in 105 kPa vacuum). It was observed that starting from a very high surface roughness for the shortest sequential DIA duration (<1 min), the roughness decreased exponentially with ongoing DIA treatment, and thereafter, the morphology slowly evolved through an intermediate multilayered island-hole structure, finally transitioning into a single-layered island-hole morphology. The AFM evaluated RMS roughness for M_n = 51 k ($R_{rms,max}$ = 7.4 nm) and 66 k ($R_{rms,max}$ = 37 nm) is plotted against the treatment time in Figure 4, where the initial and final states are well-developed lamellar morphologies for TA and DIA annealed films, respectively. These measurements were made for the samples whose AFM images are shown in Figures S4 (M_n = 51 k) and S5 (M_n = 66 k). The data was fitted to an exponential function where the smaller exponent for M_n = 66 k (0.0002 compared to 0.04 for M_n = 51 k) was consistent with the expectation that the entangled films should exhibit slower dynamics. Entanglements evidently slow down the recovery to the "equilibrium" smooth surface (or single-layered island-hole topography) from the rough surface of the nonequilibrium "transition morphology". Multilayered island-hole transitional morphologies also have a large surface area, and these structures can likewise be trapped by rapid solvent removal during the intermediate stages of the sequential DIA immersion process. This type of large surface area structure might have applications such as microporous membranes, microreactors, and large surface area electrodes.

To gain further insight into this type of surface pattern formation process, AFM was utilized to locate and scan a specific location of a thermally annealed film's island-hole morphology subjected to sequential DIA treatments. The exact film location was scanned after each annealing step to track the development and reorganization of the surface features. These locations were marked by lines on the sample surface, and scans were performed at the center of these marked regions. As the film only swells and is pinned to the substrate due to a PMMA wetting layer, the position of the lines does not change with successive DIA steps. After very short DIA treatment and drying (<1 min) of a BCP film with M_n = 51 and 66 k, we found the films rapidly swelled and an interesting growing wrinkling pattern in the outer lamellar layers formed (as seen in the AFM measurement of the dry film) without significantly disrupting the lateral molecular structure (arrangement of polymer chains in the plane of the film). AFM scans of these wrinkling patterns in Figure S4 of Supporting Information show that for DIA treatment on the TA-ordered PS-*b*-PMMA (M_n = 51 k) film, the original island-holes structures (TA microstructures) remain distinguishable within the wrinkled transition morphology. After a long DIA time (2 h), this transient structure "heals" back to the regular parallel lamellar structure as found for ordinary DIA annealing with essentially the exact island-hole boundaries but reduced domain size ($1L_{o,DIA}$).

Collectively, these observations suggest that the film restructuring occurs simultaneously at all domain interfaces of the lamellae and produces multilayered island-hole topography and then a regular single-layered lamellar surface morphology without any lateral chain rearrangement, at least on the surface. Therefore, the transition mechanism for low M_n BCPs involves rapid chain diffusion perpendicular to the substrate, much faster than lateral chain diffusion. When the above treatment is repeated for a BCP with M_n = 66 k (Figure S5), the island-hole boundaries of the initial TA (at 180 °C for 24 h) structure remain intact for up to 30 min of sequential DIA before the lateral chain diffusion becomes significant, suggesting a slower perpendicular chain diffusion by DIA compared to low M_n BCPs. Due to the slow chain dynamics of high M_n BCPs, the original TA surface topography gets completely disrupted due to lateral and perpendicular chain diffusion as the rough intermediate morphology evolves with increasing DIA time.

Effects of Film Thickness Commensurability and Block Volume Fractions on Surface Pattern Formation. On careful examination of the AFM data, regions with island-hole topography develop wrinkles differently compared to flat, commensurate film thickness surfaces, wherein commensurate refers to films with thicknesses that exhibit a smooth surface with a long-time TA equilibrium state. To identify and analyze the origins and differences in film disruption with respect to film surface topography (both with and without islands-holes), PS-*b*-PMMA (66 k) film was cast with a continuous thickness gradient using flow coating, wherein commensurate and incommensurate thickness are present in a seamless continuous manner across the thickness range for a careful study of transition regions.[32,46] They were treated with the same sequential annealing treatment of TA + DIA. On equilibration by TA at 180 °C for 24 h, the films developed island-hole morphologies in the incommensurate areas of the film. Based on the degree of thickness incommensuration calculated simply as a percentage deviation from a starting commensurate thickness, two distinct island-hole heights were observed. For

https://doi.org/10.1021/acsami.4c00068
ACS Appl. Mater. Interfaces 2024, 16, 15569−15585

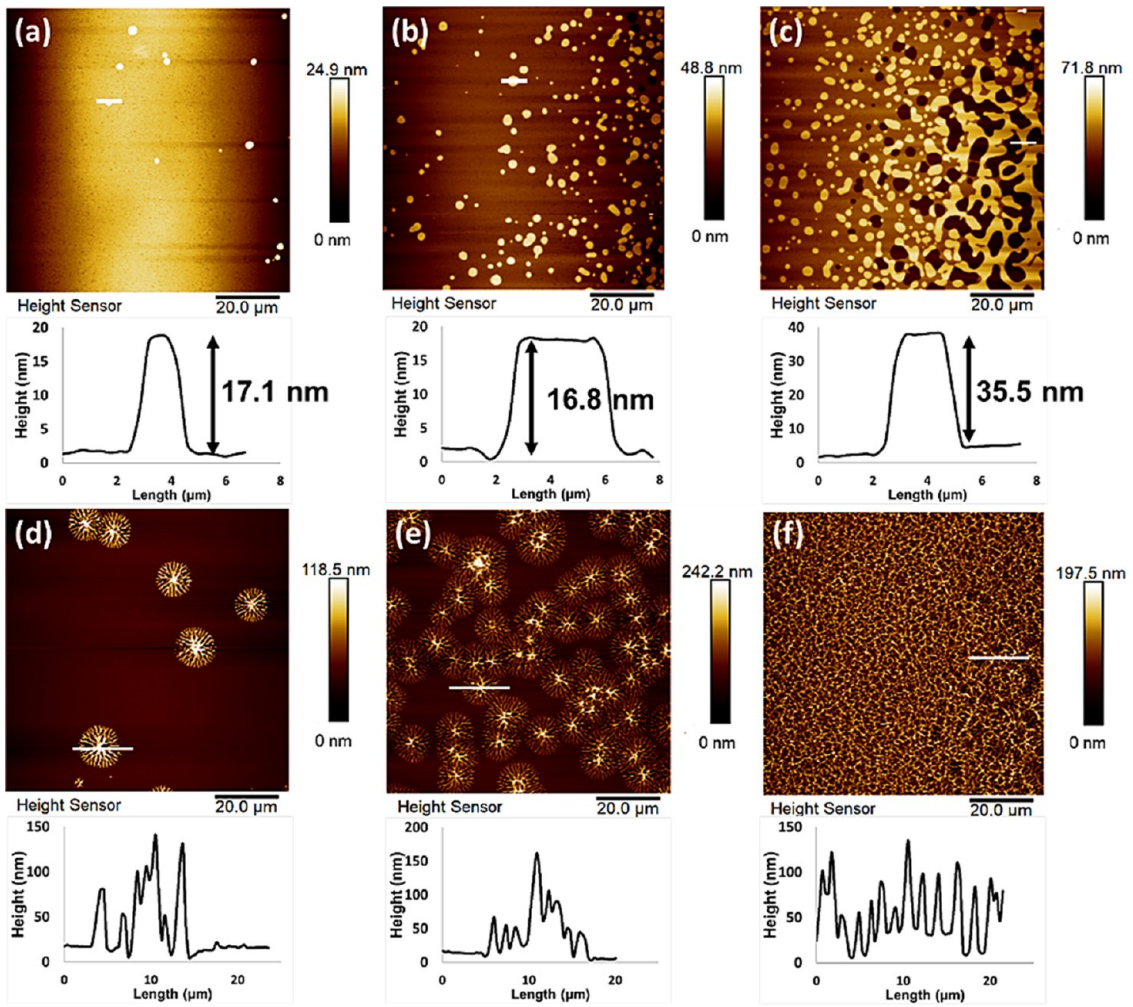

Figure 5. AFM height sensor images and line height profiles for PS-*b*-PMMA (33k-*b*-33k) films with a thickness gradient of 80 to 110 nm annealed via TA at 180 °C in a vacuum for 24 h for (a) commensurate film thickness, (b) partially commensurate film thickness, (c) incommensurate film thickness, and films annealed sequentially via DIA in SM_1 for 15 s, (d) commensurate film thickness, (e) partially commensurate film thickness, and (f) incommensurate film thickness. The numerical in the line height profiles are heights in nm.

instance, as the degree of incommensurability increased from 7 to 22% for the AFM scans in Figure 5a−c, the island-hole heights increased from $\approx 0.5L_{o,TA}$ to $1L_{o,TA,}$ indicating that the near commensurate regions produce islands-holes with smaller heights due the lack of a sharp thickness change.[34,47] These films were then sequentially annealed in SM_1 for just 15 s to capture the most rapid microstructure transformation induced due to solvent absorption and wrinkling. The second row in Figure 5 shows AFM height sensor scans for the surface morphology observed on dried films after subsequent DIA. For the region of the film with a lower degree of incommensuration, starburst-like patterns develop on the film surface and on the $0.5L_{o,TA}$ island-holes, indicating that the wrinkling instability nucleates locally in regions with defects where the solvent is first absorbed. Where the island-hole topography is fully developed, similar wrinkles first appear at the boundary of these topographical features, suggesting that solvent uptake begins at these boundaries. The growth of this instability was tracked with sequential DIA time for films (M_n = 66 k) with and without the island-hole topography (incommensurate and commensurate regions, respectively) by performing AFM after each DIA annealing step at precisely the same location using the same procedure of marking lines on dry films. The wrinkle evolution for the island-hole surface could be tracked from the boundaries of these topographical features. For TA-annealed surfaces that are smooth, AFM tracking could be done after the nucleation of a starburst-like wrinkle pattern and then following its growth. The stepwise solvent immersion and drying process has very little effect on the self-assembly process, evident from similar growth patterns observed in situ using optical microscopy. Due to the rapid nature of the wrinkling process, the stepwise method was the only way to track the topographical growth using AFM. Figures S6 and S7, respectively, show how the local bursts of wrinkling patterns (starburst-like features for a near commensurate thickness) and those at the boundary of the island holes grow with DIA treatment time and cover the entire surface and depth of the film before any reorganization (surface healing) can begin. As the wrinkles grow not only laterally but also out of the plane, we observe an instantaneous increase in surface roughness for the shortest sequential DIA durations, beyond which the roughness decreases exponentially with extended DIA, and the film's surface regains the single-layered island-hole morphology with reduced domain sizes ($L_{o,DIA}$). We see that for the initially incommensurate region of the TA-ordered film for the same treatment times, the surface still has a multilayered lamellar

https://doi.org/10.1021/acsami.4c00068
ACS Appl. Mater. Interfaces 2024, 16, 15569−15585

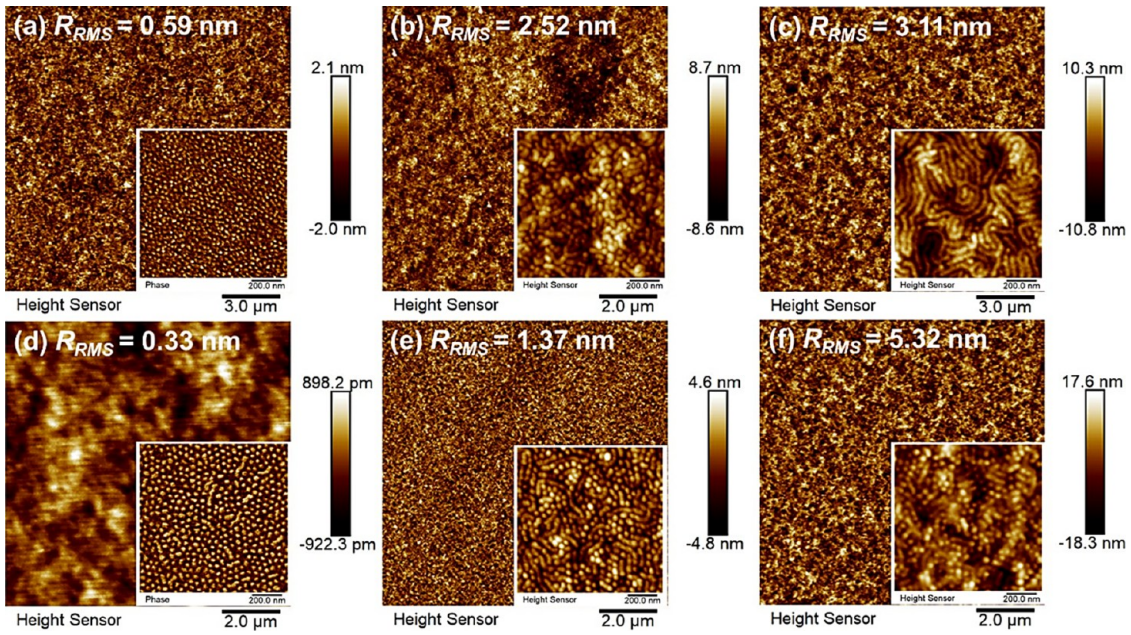

Figure 6. AFM height sensor and phase images for PS-*b*-PMMA (55k-*b*-22k) films, corresponding to a cylindrical volume fraction for, (a) As-cast; (b) DIA in SM1 for 5 s; (c) DIA in SM_1 for 1 h; (d) TA at 180 °C for 24 h; (e) TA at 180 °C for 24 h, followed by DIA in SM_1 for 5 s; and (f) TA at 180 °C for 24 h, followed by DIA in SM_1 for 1 h.

structure (Comparing panels (k) and (l) for Figures S6 and S7). After the same DIA time, the TA-ordered commensurate region has developed single-layer island-hole topography, suggesting that the film's surface heals faster when initially smooth.

A detailed analysis of the initial wrinkling pattern in a TA-commensurate film is shown in Figure S8, with 3D visualizations and line-height profiles showing that the magnitude of surface instability can be large, starting from fully TA-ordered films. The rapid evaporation of the solvent from the film on removal from the bath can produce enhanced roughness on the surface. To confirm that wrinkling occurs during solvent absorption and is not a result of solvent evaporation, optical microscopy was used to track the development of the wrinkling pattern on a smooth surface (commensurate TA thickness) in situ. Upon solvent addition, a short time (seconds) is required to refocus the sample and we observe wrinkles nucleating at multiple point sites (possible defects on the surface) that grow, merge, and cover the entire film surface. The growth stops as soon as the solvent evaporates. The videos were enhanced and slowed down to observe the growth of individual wrinkles (link in web version; Video S1).

To delve further into the origins and development of the wrinkling instability produced by sequential DIA that disrupts nascent lamellae formed by TA and to potentially control it, films of BCP with M_n = 66 k were thermally annealed for very short durations at relatively high T (180 °C), followed by DIA for a conventional treatment time of 45 to 60 min, enough to order a disordered as-cast film entirely. The analysis, shown in Figure S9, revealed that a fully developed TA microstructure is not required to disrupt the film surface on the secondary DIA immersion. We observed that only a few min of TA was sufficient to produce some degree of segregation and stratification into PS and PMMA layers and could disrupt the transition and slow down the usually rapid DIA process. For instance, a film annealed first by TA for only 15 min would produce an underdeveloped rough transition morphology after 45 min of DIA treatment. The transition morphology is underdeveloped in the sense that it has a much lower surface roughness compared to a film annealed by TA for 24 h (fully developed) followed by 45 min of DIA. As a result of the lower surface disruption, the time required to recover the DIA microstructure is reduced to only 2 h of sequential annealing. The initial segregation of PMMA and PS into parallel domains occurs very quickly on high-temperature TA,[48] which is sufficient to produce a swelling mismatch and wrinkling on sequential DIA. This initial segregation was measured using time-of-flight secondary ion mass spectroscopy for short-time TA annealed films (Figure S10a). Within only 1 min of TA, the segregation of PS to the surface and PMMA to the substrate is observed, and in 30 min, some degree of TA lamellar layer development can be observed. With an extended first TA process, lamellar morphology develops sharp interfaces throughout the film thickness, which constrains isotropic chain swelling when submerged into the solvent mixture, enhancing the amplitude of the surface wrinkles. Figure S10b plots film RMS roughness for short-time TA and after a subsequent fixed time (45 min) DIA. The plot shows that after TA lamellar layers have started developing inside the film, sequential DIA produces a very rough surface after film drying.

Besides a lamellar BCP, we subjected a cylinder-forming BCP to a sequential TA + DIA process and found that the wrinkled transition states do not exist for these BCP volume fractions. To understand the morphology dependence (affected by block volume fractions) of these transition pathways for asymmetric BCPs, PS-*b*-PMMA (55k-*b*-22k) films with a cylindrical block volume fraction were treated via sequential TA + DIA. Figure 6 shows the AFM analysis for these films. The as-cast film shows only initiated microphase separation produced during solvent evaporation, and the long-time thermally annealed film has a vertical cylindrical morphology on the surface, likely due to kinetic trapping of the entropically favorable orientation or to reduce the surface

https://doi.org/10.1021/acsami.4c00068
ACS Appl. Mater. Interfaces 2024, 16, 15569−15585

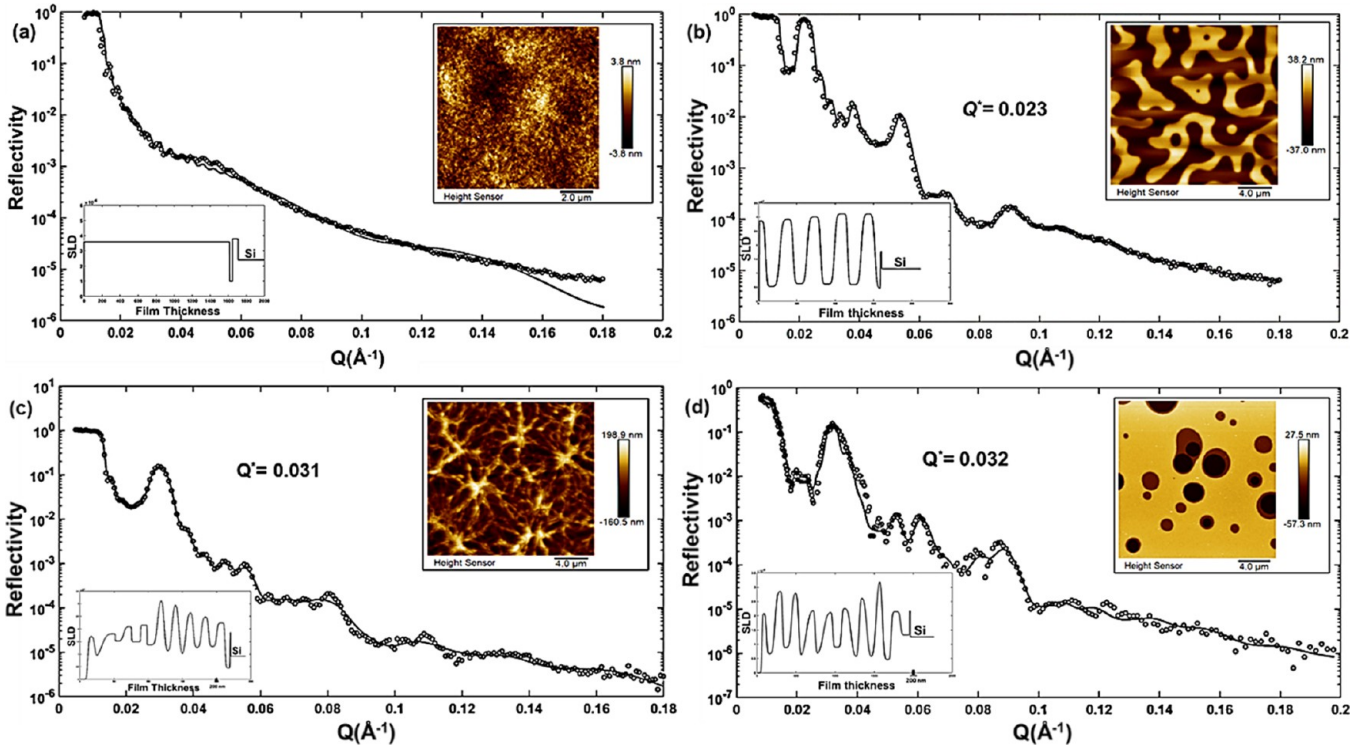

Figure 7. Neutron reflectivity data (o) and fits (−) along with scattering length density profiles (bottom left) for *sym* dPS-*b*-PMMA (M_n = 62 k) films and corresponding AFM height sensor images. (a) As-cast film; (b) film thermally annealed at 180 °C for 24 h; (c) film thermally annealed at 180 °C for 24 h followed by DIA in SM_1 for 30 min; and (d) film thermally annealed at 180 °C for 24 h followed by DIA in SM_1 for 48 h. The values for Q^* in the inset are the positions of Bragg's peaks.

area by preventing curvature on the film surface from parallel cylinders. On subsequent DIA annealing, no significant surface roughness/instability was observed for this cylindrical microstructure. Large area scans show some roughness enhancement post-DIA, which was observed for DIA on both as-cast and TA-treated films. Also, the surface roughness, although higher than that for as-cast or TA annealed samples, is nowhere close to the scale arising in association with wrinkling pattern formation in a lamellar film under the same treatment conditions.

High-resolution scans for the same cylindrical BCP samples shown as insets in Figure 6 reveal that films with TA-ordered cylinders do not wrinkle on subsequent DIA. The cylindrical morphology was found to have better parallel orientation for a film DIA treated from the as-cast disordered state compared to those with an initial TA order, which showed a mixed morphology (parallel and perpendicular) after the sequential treatment of 1 h DIA. It can be seen from Figure 6e,f that more cylinders become parallel on extended DIA. These AFM results suggest that some out-of-plane symmetry breaking (as in the case of parallel lamellae) is needed for differential layer swelling that can produce wrinkling instability. In addition to a sequential solvent immersion process, TA-ordered films were subjected to sequential solvent vapor annealing. The transition morphologies, mechanisms, and kinetics are discussed in brief in the SI and in Figures S11−S13.

Analyzing Interior Lamellar BCP Film Morphology with Neutron Reflectivity. Neutron reflectivity was performed on a partially deuterated *sym* BCP of dPS-*b*-PMMA (M_n = 62 kg/mol) to have a reference for individual TA and DIA internal morphologies. The primary and secondary scattering peaks were obtained at wave vector transfer values (Q values) of 0.23 $Å^{-1}$ (×1) and 0.38 $Å^{-1}$ (≈ ×2), respectively, for a thermally annealed film and confirmed parallel lamellar microstructure. The same values for a DIA annealed film were observed at Q values of 0.34 $Å^{-1}$ (×1) and 0.63 $Å^{-1}$ (≈ ×2). The domain size is inversely proportional to the position of the primary Bragg peak and is obtained by fitting the NR data to a linear SLD profile.

Figure 7 shows the neutron reflectivity data along with respective fits to a linear model that gives SLD variations with film depth. The SLD after deuteration is enhanced, and therefore, the SLD profiles have higher values where the density of dPS chains is higher along the film depth (dPS layer SLD ≈ 6×10^{-6} $Å^{-2}$ compared to the PMMA layer SLD ≈ 1×10^{-6} $Å^{-2}$). The SLD undulations directly correlate to PS and PMMA variations along the film depth. NR for as-cast films does not show a Bragg peak, but only high-frequency Kiessig oscillations corresponding to the total film thickness.[49] Thermally annealed films show well-developed alternating layers of dPS and PMMA with an average domain size of 35 nm ($L_{o,TA}$) in the form of an oscillating SLD profile. The NR fits and SLD profiles are presented in Figure 7, along with AFM images (inset) of the surface topography for M_n = 66 k films processed with the same treatment procedure. The NR samples were chosen to have commensurate/very near commensurate thickness to produce a smooth surface for NR measurements. However, due to the large area of samples, the formation of islands-holes cannot be eliminated. Further, due to a discrepancy in the domain sizes, it is difficult to identify a thickness commensurate with the periodicities for both TA and DIA.

The SLD for air is essentially zero, followed by a high SLD layer confirming the presence of dPS on the film surface. The

https://doi.org/10.1021/acsami.4c00068
ACS Appl. Mater. Interfaces 2024, 16, 15569−15585

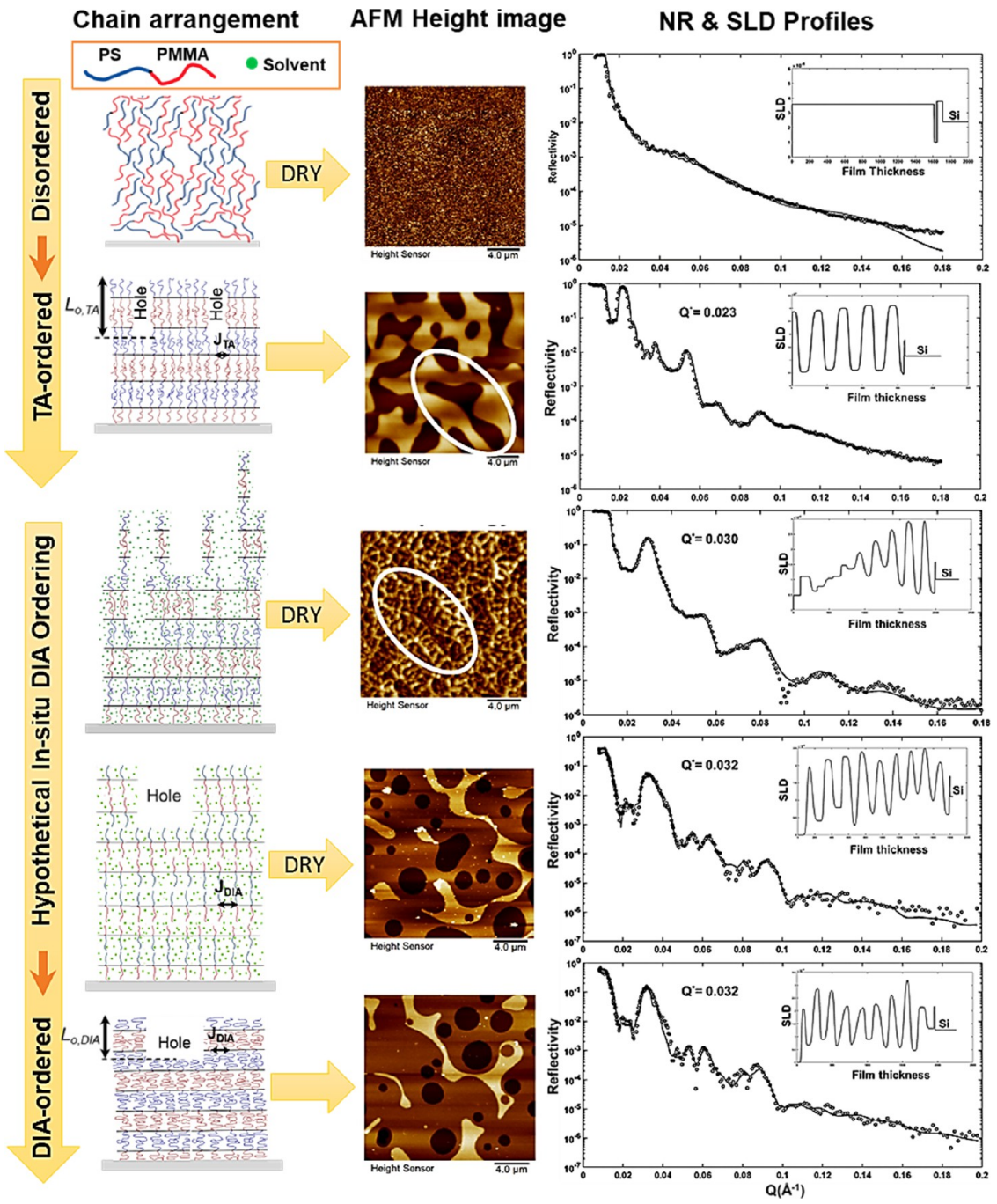

Figure 8. Proposed chain rearrangement mechanism from a thermally annealed microstructure of stretched chains to the trapped DIA annealed transition microstructure. AFM height sensor images in the inset show the retention of original island-hole morphology (circled) in thermally annealed PS-*b*-PMMA (M_n = 66 k) films successively annealed via DIA for 10 min. At longer sequential DIA times, chain rearrangement occurs both parallel and perpendicular to the film causing a complete transformation of the film surface topography along with the domain size. The SLD profile in the extreme right shows damped oscillations near the air interface where the polymer chains are nonuniformly distributed.

lower SLD for the layer at the air interface compared to the SLD of a fully deuterated layer is likely due to the island-hole topography on the film samples. The rightmost end of the SLD profile corresponds to a thin silicon oxide layer (SLD ≈ 3.4 × 10^{-6} Å^{-2}) followed by the Si substrate. The layer left to this silicon oxide layer has a low SLD due to the migration of the PMMA block. NR performed on thermally ordered films after successively treating with short-time (30 min) DIA is presented in Figure 7c and shows damped SLD oscillations near the air−polymer interface corresponding to the highly roughened top surface of the wrinkled morphology. In the middle of the film, the SLD profile shows a gradient in layer thicknesses from a reduced domain size of approximately 20 nm (≈ 0.55$L_{o,TA}$) in the middle to a higher value of 23 nm (≈ 0.7$L_{o,TA}$) near the substrate. The layers near the film surface swell first and are more swollen relative to those near the substrate before the swelling becomes isotropic. Therefore, there is a higher reduction in domain size on solvent evaporation for layers near the film surface compared to those near the substrate. The higher value is, i.e., the remnant

https://doi.org/10.1021/acsami.4c00068
ACS Appl. Mater. Interfaces 2024, 16, 15569−15585

domain order from the initial TA process. The damped oscillations for the transition morphology near the film's surface suggest the presence of some order (transient alternate layers of dPS and PMMA) under the undulating surface features driven by immersion and swelling of the TA-ordered lamellar layers in the DIA solvent mixture. The SLD profiles and fitted data for films annealed with an extended DIA time of 48 h (Figure 7d) show well-developed oscillations in the SLD with an average domain size of 25 nm ($\approx 0.8L_{o,TA}$) throughout the film. NR was also performed at the intermediate stages of morphological evolution, and the results are presented in Figure S14. For the 48 h annealed film, domain size is higher than short time annealed as 48 h is sufficient for complete chain reorganization, producing a lamellar structure with a better degree of domain segregation and lower interfacial widths.

Origins and Growth of Swelling-Induced Wrinkling Patterns. Successive DIA on a pre-thermally annealed lamellar structure causes the ordered film to swell instantaneously on immersion in the solvent mixture. This rapid swelling only occurs perpendicular to the plane of the film because swelling in the lateral direction is restricted by the pinning of the film onto the substrate due to the preferential interaction between the PMMA layer segregated to the substrate and the SiO_x present on the substrate surface. However, this rapid solvent absorption is not isotropic and swells the top and bottom layers differently. As the solvent diffuses in and swells the bottom PMMA layer more than PS (due to acetone selectivity for PMMA) in the domain near the film surface, the volume expansion mismatch between parallel layers results in film buckling and wrinkling on very short solvent immersion times (minutes). The initial sources of solvent incursion into the film can be tracked to point defects (leading to starburst-like wrinkling pattern growth) on a smooth commensurate surface and to the boundaries of TA-produced islands-holes (leading to wave-like wrinkling) for incommensurate film thicknesses. With relatively longer immersion times, the wrinkles grow out to cover the entire film surface and the full depth of the film, disrupting it altogether. We hypothesize that after sufficient solvent absorption, the highly swollen BCP chains push against each other at every TA-ordered interface, and the stresses exude chains perpendicular to the substrate to form new layers near the polymer−air interface. With extended DIA (many hours for high M_n BCPs), the swelling becomes more uniform, allowing the chains to diffuse, overcome entanglements, and order into the enthalpically stable solvent swollen parallel lamellae. Initially, all the layers are not uniformly formed as the starting point is a completely disrupted film, and we see a multilayered island-hole topography due to rearrangement happening at every interface. The microstructure eventually heals to a swollen single-layered island-hole surface morphology with a large chain junction spacing (J_{DIA}) that gets trapped on rapid solvent evaporation to produce shrunken lamellar layers with a collapsed chain configuration ($L_{o,DIA}$) in dry films. The schematic in Figure 8 describes this hypothesis. The wrinkling hypothesis is also supported by the presence of dampened oscillations near the air interface in the fitted SLD profiles for these films, indicating that the film initially only wrinkles with the TA-ordered dPS and PMMA layers somewhat intact. The average SLD contrast between layers is reduced (dampened) due to the presence of air along with the polymer in the surface wrinkles. SLD profiles for very short DIA treatments on thermally equilibrated films presented in Figure S14 show the rapid increase in the number of layers within the first few min of treatment with damped SLD oscillations (Figure S14b,c), eventually leading to surface wrinkling (Figure S14d,e) and then complete film disruption (Figure S14f) with more DIA time. The short-TA + conventional-DIA treatments revealed that a fully formed precursor lamellar morphology is not required, and even initially segregated surface layers are enough to disrupt the film on subsequent DIA. Also, such instability does not exist for cylinder-forming BCP films. The differences between lamellar and cylindrical BCPs suggest that any degree of symmetry breaking can cause differential expansion and produce wrinkle pattern and that this symmetry breaking needs to be out of the plane of the film. The degree of segregation into lamellae affects the magnitude of disruption and is related to the increasing rigidity of the structure with increasing segregation (increasing sharpness of the interfaces).

Tracking the growing wrinkle diameter for starburst-like patterns shows a linear trend vs immersion time with a slope of approximately unity, 1 (Figure S3). This linear trend has been observed by Chung et al. for wrinkle pattern growth on PS films with cross-linked surfaces[41] and also for spherulitic growths in semicrystalline isotactic polystyrene films.[43] We further observed that wrinkle pattern growth does not instantaneously start and there is a small induction time of approximately 3 s for the data shown in Figure S3. Such induction times have been reported in contexts of frontal photopolymerization and propagating waves of network formation in polymerizable liquids.[50,51] Small induction times (minutes) have also been observed for wrinkling growth on surface cross-linked PS films by Chung et al. for radial target-like patterns along with linear growth. The temporal (seconds) and spatial (nm) scaling is much smaller for wrinkling of ordered BCP films compared to previous studies, as the solvent absorption is almost instantaneous with high proportions of swelling solvents in the immersion mixture.

The rough surface transition morphology necessitated an extended time for the material to rearrange into regular lamellar layers. This trend was evident as the molecular mass increased from 51 to 66 k, where this time increased from minutes to days. The multilayered island-hole morphology observed during this transition suggests simultaneous chain rearrangement at multiple fronts/lamellar interfaces. This rough transition morphology is not observed for short DIA treatments on as-cast disordered films because the swelling of randomly trapped as-cast chains is isotropic, and only an overall film thickness increase has been observed via ellipsometry.[13] Upon isotropic swelling, chains are highly mobile and attain a parallel layered structure of chains oriented perpendicular to the substrate with larger junction spacing (J_{DIA}) than that in the melt (J_{TA}). A similar sequential swelling mechanism applies to the sequential TA + SVA treatment of BCP films, where the swelling is driven by solvent vapor incursion instead of the liquid solvent mixture.

Molecular Mass Effects on Morphology Transition Kinetics. To understand the relatively slow dynamics of the high molecular mass BCPs, such as M_n = 66 and 89 k, compared to low molecular mass BCPs (M_n = 36.5 and 51 k), we consider a simple entanglement model. The entanglement molecular mass ($M_{e,dry}$) values for PS and PMMA in the melt state are, for comparison, equal to 18.5 and 10 k, respectively.[13] The entanglement molecular mass of a homopolymer swollen

https://doi.org/10.1021/acsami.4c00068
ACS Appl. Mater. Interfaces 2024, 16, 15569−15585

by a solvent in a solvent-swollen material ($M_{e,s}$) has often been found to be described by,[52−55]

$$M_{e,s} = M_{e,dry}\varphi^{-\alpha} \quad (1)$$

where φ is the polymer volume fraction of the polymer solution, $M_{e,dry}$ is the entanglement molecular mass in the absence of solvent, and α is a scaling exponent describing the "strength" of the concentration dependence of the entanglement molecular mass. The value of α is often observed to be in the range of 1 to 4/3 for solutions of linear flexible polymers in solution, in agreement with the theoretic predictions for concentrated polymer solutions and semidilute polymer solutions in a good solvent, respectively.[56] For the purposes of our qualitative discussion of entanglement in BCP solutions, we simply assume that this same relation applies as a rough approximation. For example, by taking a polymer concentration with φ = 0.56 and α = 4/3, we estimate the modified entanglement molecular mass for homopolymer PS and PMMA to be 28 and 21 k g/mole, respectively. The proximity of these approximate estimations to the BCP with PS and PMMA block masses of 25 and 26 k, respectively, suggests that entanglements may significantly affect the reorganization kinetics. While Figure 8 describes chain reorganization for entangling polymers, we have attempted to show a different non-entangling mechanism for low molecular mass BCPs in Figure S15.

Here, the rapid perpendicular chain diffusion preserves the original TA island-hole topography, causing only a reduction in layer thickness on rapid chain collapse. Similar dilution effects should apply to the cascaded TA + SVA process; however, the dynamics may also be affected by the lower swelling in vapor, leading to poor instability in the films coupled with poor chain diffusion.

Energy Landscape Rationalization of Pattern Formation. These changes in the surface morphology can be formally described by an abstract free energy diagram (Figure 9) based on the surface and interfacial areas/energies of the morphologies observed. The disordered as-cast state should have the highest free energy because of the large number of unfavorable contacts between unlike polymer chains in this highly nonequilibrium state. At the other extreme of free energy, the thermally annealed (TA) BCP morphology should correspond to the equilibrium morphology having the lowest free energy and the minimum interfacial area. The metastable DIA microstructure should have intermediate free energies to these extreme film states. Our group derived specific free energy estimates for these states in a previous publication based on the Turner and Walton models for estimating the free energy of this type of BCP material.[57−60] The same procedure is repeated here, and the results are presented in the SI. As one would naturally expect, the transitional morphologies have free energies greater than the metastable DIA morphology but lower than the disordered state. The higher energies of the transition morphologies are due to the disruption at the film surface that leads to a large increase in the surface area compared to the material in its relatively ordered metastable DIA-generated state. The transition state energy is lower than the completely disordered film because the films retain some order near the substrate and within the wrinkles, as confirmed by the fitted NR data. The red curve in Figure 9 describes the system starting from an initial disordered state of high free energy. On TA treatment, the material passes through a high activation energy barrier related to the reduced incompatibility (χ) in the high-temperature thermal melt. There are also kinetic processes impeding this transition. This activation peak in the free energy (ΔE_1) is required to overcome the diffusion barriers for the initial segregation of PMMA chains to the SiO_x substrate and PS chains to the air interface.

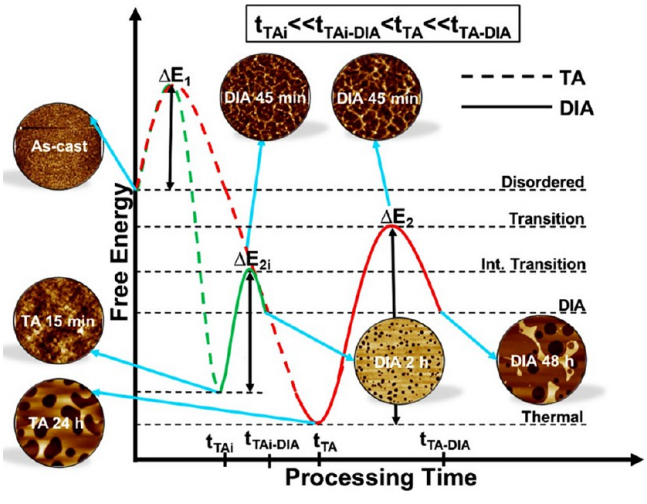

Figure 9. Schematic free energy diagram showing transitions from disordered to TA and further to DIA microstructures. The AFM images show the surface structure at each energy minima and maxima. ΔE represent activation energy requirements and t on the time axis represents the difference in relative processing times.

Beyond this stage of evolution for the system on its energy landscape, the structural evolution of the BCP film can be expected to be enthalpically driven by layer segregation. After the TA processing, the morphology settles into the ordered equilibrium state or a state close to this condition. On sequential DIA processing, however, the BCP interfacial structure becomes destabilized, and the system "jumps" to a new higher free energy state because of the creation of extra surface area. Evidently, the formation of this microstructure requires considerable activation energy (ΔE_2) compared to conventional DIA. After a sufficient DIA treatment time, the BCP interfacial structure transforms into a metastable DIA morphology. The green curve considers an evolution involving intermediate morphologies. The system again starts from the disordered state of the cast film. After a short time of TA processing, the ordering process initiates at the polymer−air, and polymer−substrate interfaces due to preferential PMMA and PS segregation. Nonetheless, the system does not reach the lowest energy equilibrium state due to limited processing time (confirmed using ToF-SIMS depth profiling). On successive DIA processing steps of these partially ordered films, the surface becomes disrupted again, although the magnitude of this disruption (RMS roughness) is much lower. Thus, to traverse through the transition morphology for these intermediate free energy structures, the activation energy requirement (ΔE_{2i}) for reassembly is reduced. For these poorly ordered intermediate structures, the metastable DIA morphology is obtained in a much shorter time as the intermediate state from which the system recovers is at a relatively lower free energy level.

CONCLUSIONS

This article has conveyed information and analysis for microstructure transitions in block copolymer films for

https://doi.org/10.1021/acsami.4c00068
ACS Appl. Mater. Interfaces 2024, 16, 15569−15585

sequential thermal and direct solvent immersion annealing. The sequential treatment pushes the system from an equilibrium low interfacial energy state through a high surface energy (large surface area) intermediate morphology, which is pathway-dependent, to a metastable higher interfacial free energy (compared to that achieved by TA) microstructure on long-time DIA. The properties discussed include BCP molecular mass that affects transition kinetics due to the introduction of chain entanglements, degree and type of structure formation that controls the wrinkling instability on sequential DIA, and solvent mixture quality (solubility parameter) and state (liquid vs vapor) that controls DIA/SVA kinetics. Sequential DIA on a thermally annealed structure showed rapid swelling and wrinkling of the pre-existing parallel lamellar structure due to differential swelling of the blocks, where the wrinkling pattern intensity and coverage can be controlled by BCP molecular mass (or domain size) and DIA processing time, respectively. The rapid wrinkled morphology grows linearly with immersion time. It slowly transitions into a multilayered island-hole morphology due to chain rearrangement at all TA interfaces before achieving a regular DIA lamellar structure, and the BCP molecular mass governs the kinetics. Chain entanglements significantly influence the rate at which these free energy barriers are crossed. In particular, BCPs having a mass greater than their estimated entanglement molecular mass exhibit much slower dynamics, which can cause the material to be "frozen" in a nonergodic nonequilibrium state. We further find that any pre-induced out-of-plane symmetry breaking (formation of parallel lamellae) by using a brief period of TA processing can disrupt the film surface upon subsequent DIA processing steps. The extent of initial TA ordering controls the nature and magnitude of the observed surface pattern and the slowing down of the ordering rate associated with the system having to climb up the free energy landscape in which it is trapped to resume its evolution to its lowest free energy state. The rough/wrinkled transition morphology and the multilayered island-hole morphology arising from this process can be observed by vitrifying the film through quick solvent removal at any intermediate stage of the sequential DIA step. The process gives rise to structures for use in various applications requiring large surface areas, such as membranes, catalysis, and biomass growth, once the film structure is "stabilized" by cross-linking or "enhanced" by selective etching. Our work demonstrates the potential of utilizing nonequilibrium processing treatments to navigate the free energy landscape and achieve target morphologies that cannot be achieved under equilibrium conditions for diverse applications.

EXPERIMENTAL SECTION

Experimental Design. Thin films of a diblock copolymer were cast on silicon substrates and annealed in thermal, solvent mixtures, and solvent vapor environments. The processing conditions (time, temperature, solvent mixtures, etc.) were chosen to identify an optimal sequential treatment to explore the BCP morphology evolution and self-assembly.

Materials. The polystyrene-*b*-poly(methyl methacrylate) (PS-*b*-PMMA) diblock copolymer was acquired from Polymer Source Inc. with overall number-average molecular mass of M_n = 36.5 k (19.5k-*b*-17k), 51 k (25k-*b*-26k), 66 k (33k-*b*-33k), 77 k (55k-*b*-22k), and 89 k (45k-*b*-44k) g/mol. Deuterated Polystyrene-*b*-Poly(methyl methacrylate) (dPS-*b*-PMMA) where only the PS block was deuterated with M_n = 62 k (32.5k-*b*-29.5k) g/mol was also obtained from Polymer Source Inc. All block volume fractions correspond to a symmetric diblock (volume fraction of PS ≈ 0.5) except for the diblock with M_n = 77 k which has a cylindrical volume fraction. BCP solutions were made in laboratory-grade toluene (VWR BDH Chemicals, ACS reagent, ≥99.5%) with a 3 to 5% concentration. Direct immersion annealing and solvent vapor annealing were performed in sealed glass jars. The solvent mixtures (SM) are composed of Heptane (VWR BDH Chemicals, Laboratory reagent, ≥99.9%), Acetone (VWR BDH Chemicals, ACS reagent, ≥99.5%), and Toluene (VWR BDH Chemicals, ACS reagent, ≥99.5%). Heptane is a poor solvent for PS and PMMA, while toluene is a good solvent for both. Acetone has more selectivity toward PMMA due to its polar nature.[13,19]

BCP Thin Film Preparation. Thin films were cast from solutions of PS-*b*-PMMA of different molecular masses and dPS-*b*-PMMA in toluene using the flow coating method. This method requires only minute quantities of the polymer solution. The polymer solution was pipetted into the gap between an angled glass blade and a flat Si substrate (substrate is Ultraviolet Ozone (UVO)-treated for 120 min). The blade edge moved along the substrate, pulling the bulk of the solution along with it and coating a thin layer onto the substrate. Films were also prepared using a standard spin coating method to confirm the effects of the film coating technique on the sequential treatment.

Annealing Treatments. DIA was done in sealed glass jars at room temperature (≈ 25 °C). The solvent mixture comprised heptane, acetone, and toluene in the solvent mixture (*SM*) proportions of SM_1 = 75:25:5, and SM_2 = 60:30:10 by volume fractions, respectively. The composition SM_1 has been reported to be optimum for low M_n lamellar PS-*b*-PMMA by Longanecker et al. The concentrations of the good solvents were increased or decreased relative to SM_1 to expedite assembly for high M_n BCP films or to prevent dewetting of low M_n BCP films. Here, heptane is a nonsolvent for both PS and PMMA, toluene is a neutral good solvent for both, and acetone is a selective good solvent for PMMA. DIA immersion times were also varied with the BCP molecular mass for any particular SM. Conventional DIA times as per original research are 30 to 90 min and may vary with M_n. These durations were found sufficient to fully order BCP films from a disordered as-cast state. All films were heated on a hot plate at 60 °C for 5 to 10 min to remove any residual solvent post-DIA. Some films were also dried in a vacuum (≈ 100 kPa vacuum) oven at 80 °C for 24 h to check for the effects of residual solvent. Experiments for Figure 2 were conducted in a sequence; TA anneal, and AFM scan followed by DIA, drying and AFM scan followed by DIA, drying and AFM scan, and so on for the next DIA steps.

Solvent vapor annealing was done in sealed glass jars at room temperature (≈ 25 °C). The jar volume is ≈70 mL and the solvent bath volume is ≈5 mL. The films were placed on a stage ≈1 cm above the solvent bath surface, and annealing times varied from a few minutes to a few hours. The solvents studied include acetone, THF, and solvent mixture 1, also used for DIA of intermediate M_n BCPs. Films were dried on a hot plate at 60 °C for 5 to 10 min to remove any residual solvent.

Thermal annealing was performed in vacuum ovens at ≈100 kPa vacuum at temperatures ranging from 160 to 200 °C. All samples were quenched to room temperature (≈ 25 °C) post TA.

Characterization. Film thicknesses were measured using UV−vis interferometry on the Filmetrics LS-DT2 interferometer. The topography of the polymer−air interface for thin films was characterized using atomic force microscopy (AFM) on the Bruker AXS Dimension Icon in standard tapping mode in air. Height sensor and phase scans were obtained for all film samples. The height sensor images were flattened using Bruker Nanoscope Analysis software by the first order to fit each line individually and remove tilt. Neutron Reflectometry (NR) was performed to analyze the internal film microstructure on the NG7 Horizontal Neutron Reflectometer, available at the NIST Center for Neutron Research. The instrument has an incident neutron wavelength of 4.77 nm and an available Q range of 0.03−2.4 nm^{-1}. Film samples used for NR had a deuterated PS block. The acquired data was reduced using ReflRed software and analyzed using the REFLPAK package developed by NIST that fits

https://doi.org/10.1021/acsami.4c00068
ACS Appl. Mater. Interfaces 2024, 16, 15569−15585

the reflectivity data to a layer model of the sample. This forward-fitting method allows one to manually manipulate parameters like domain spacing, interfacial width, layer SLD, etc., to fit the NR data. The automatic fit method makes a gradient descent search through the fitting parameter space selected using a Levensburg-Marquardt nonlinear least-squares update procedure. Each iteration updates the parameter table, and at the end of the fit, it estimates the uncertainty in each parameter. Some NR experiments were performed on the LIQREF reflectometer at Oak Ridge National Laboratory to confirm internal morphologies for films successively treated with extended DIA. The instrument takes measurements in horizontal sample geometry, has a wavelength range of 2.5 to 17 Å, and an available Q range of 0.008 to 0.3 $Å^{-1}$. Optical microscopy was done using an Olympus microscope (BX-41) in reflection mode. Time of Flight Secondary Ion Mass Spectroscopy was performed using the ION TOF ToF-SIMS NCS instrument at RICE University's shared equipment authority. Films with a thickness of ≈100 nm were used for this measurement.

■ ASSOCIATED CONTENT

Supporting Information

The Supporting Information is available free of charge at https://pubs.acs.org/doi/10.1021/acsami.4c00068.

AFM images, optical images, and NR profiles for films annealed from as-cast to DIA, as-cast to TA, and TA to DIA; comparative AFM results for TA to SVA sequential annealing are available; ToF-SIMS analysis available for the initial stages of lamellar segregation by TA; and model free-energy calculations for lamellar BCP films for TA and DIA microstructures (PDF)

Optical microscopy video of growing wrinkle pattern on ordered lamellar BCP films (smooth surface) immersed in solvent; video is slowed by 0.5 times and shows starburst-like wrinkle pattern nucleating and growing on immersion in solvent mixture SM1 (AVI)

Video file 2 (AVI)

Video file 3 (AVI)

■ AUTHOR INFORMATION

Corresponding Authors

Jack F. Douglas − *Materials Science and Engineering Division, National Institute of Standards and Technology, Gaithersburg, Maryland 20899, United States;* orcid.org/0000-0001-7290-2300; Email: jack.douglas@nist.gov

Alamgir Karim − *William A. Brookshire, Department of Chemical and Biomolecular Engineering, University of Houston, Houston, Texas 77204, United States;* orcid.org/0000-0003-1302-9374; Email: akarim3@central.uh.edu

Authors

Kshitij Sharma − *William A. Brookshire, Department of Chemical and Biomolecular Engineering, University of Houston, Houston, Texas 77204, United States;* orcid.org/0000-0001-7309-5352

Maninderjeet Singh − *William A. Brookshire, Department of Chemical and Biomolecular Engineering, University of Houston, Houston, Texas 77204, United States;* orcid.org/0000-0001-8891-8454

Sushil K. Satija − *Center for Neutron Research, National Institute of Standards and Technology, Gaithersburg, Maryland 20899, United States*

John F. Ankner − *Second Target Station Project, Oak Ridge National Laboratory, Oak Ridge, Tennessee 37830, United States;* orcid.org/0000-0002-6737-5718

Complete contact information is available at: https://pubs.acs.org/10.1021/acsami.4c00068

Author Contributions

All the images/artwork/photos that appear in the manuscript and SI file, including those in the TOC graphic, were created by the authors of this manuscript. K.S.: Experiment design, experiments (AFM, NR, optical microscopy), analysis, manuscript preparation; S.K.S. and J.F.A.: Neutron reflectivity experiments and analysis; M.S., J.F.D., and A.K.: Analysis, manuscript preparation.

Funding

We acknowledge NSF DMR 1905996 for support of the research. Support from Welch Foundation via grants e-2105−20220331 and v-e-0003−20230731 is also acknowledged.

Notes

The authors declare no competing financial interest.

Certain commercial materials, software and equipment are identified to specify adequately the experimental procedure. In no case does such identification imply a recommendation by the National Institute of Standards and Technology, nor does it imply that the material or equipment identified is necessarily the best available for this purpose.

■ ACKNOWLEDGMENTS

We would like to acknowledge Dr. Tanguy Terlier at RICE University's Shared Equipment Authority for time-of-flight secondary ion mass spectroscopy experiments to measure the initial stratification of domains after a short time of high-temperature thermal annealing. The measurements at Oak Ridge National Lab (ORNL), run by University of Tennessee-Battelle Memorial Institute (UT-Battelle), LLC, were performed under Contract No. DE-AC05-00OR22725 with the US Department of Energy.

■ REFERENCES

(1) Fredrickson, G. H.; Bates, F. S. Dynamics of Block Copolymers: Theory and Experiment. *Annu. Rev. Mater. Sci.* **1996**, *26* (1), 501−550.

(2) Hahn, J.; Filiz, V.; Rangou, S.; Clodt, J.; Jung, A.; Buhr, K.; Abetz, C.; Abetz, V. Structure Formation of Integral-Asymmetric Membranes of Polystyrene-Block-Poly(Ethylene Oxide). *J. Polym. Sci. B Polym. Phys.* **2013**, *51* (4), 281−290.

(3) Lei, L.; Xia, Y.; Chen, X.; Shi, S. Long-Range-Ordered, Hexagonally Packed Nanoporous Membranes from Degradable-Block-Containing Diblock Copolymer Film Templates. *J. Appl. Polym. Sci.* **2014**, *131* (1), 1−15.

(4) Lee, J. Y.; Lee, J.; Jang, Y. J.; Lee, J.; Jang, Y. H.; Kochuveedu, S. T.; Lee, S. S.; Kim, D. H. Plasmonic Nano-Necklace Arrays via Reconstruction of Diblock Copolymer Inverse Micelle Nanotemplates. *Soft Matter* **2011**, *7* (1), 57−60.

(5) Fang, Z.; Zhu, X. Plasmonics in Nanostructures. *Adv. Mater.* **2013**, *25* (28), 3840−3856.

(6) Mistark, P. A.; Park, S.; Yalcin, S. E.; Lee, D. H.; Yavuzcetin, O.; Tuominen, M. T.; Russell, T. P.; Achermann, M. Block-Copolymer-Based Plasmonic Nanostructures. *ACS Nano* **2009**, *3* (12), 3987−3992.

(7) Hong, A. J.; Liu, C. C.; Wang, Y.; Kim, J.; Xiu, F.; Ji, S.; Zou, J.; Nealey, P. F.; Wang, R. L. Metal Nanodot Memory by Self-Assembled Block Copolymer Lift-Off. *Nano Lett.* **2010**, *10* (1), 224−229.

(8) Singh, M.; Agrawal, A.; Wu, W.; Masud, A.; Armijo, E.; Gonzalez, D.; Zhou, S.; Terlier, T.; Zhu, C.; Strzalka, J.; Matyjaszewski, K.; Bockstaller, M.; Douglas, J. F.; Karim, A. Soft-Shear-Aligned Vertically Oriented Lamellar Block Copolymers for Template-Free Sub-10 Nm Patterning and Hybrid Nanostructures. *ACS Appl. Mater. Interfaces* **2022**, *14* (10), 12824−12835.
(9) Liu, W.; Chen, J.; Zhou, D.; Liao, X.; Xie, M.; Sun, R. A High-Performance Dielectric Block Copolymer with a Self-Assembled Superhelical Nanotube Morphology. *Polym. Chem.* **2017**, *8* (4), 725−734.
(10) Samant, S.; Basutkar, M.; Singh, M.; Masud, A.; Grabowski, C. A.; Kisslinger, K.; Strzalka, J.; Yuan, G.; Satija, S.; Apata, I.; Raghavan, D.; Durstock, M.; Karim, A. Effect of Molecular Weight and Layer Thickness on the Dielectric Breakdown Strength of Neat and Homopolymer Swollen Lamellar Block Copolymer Films. *ACS Appl. Polym. Mater.* **2020**, *2* (8), 3072−3083.
(11) Sharma, K.; Agrawal, A.; Masud, A.; Satija, S. K.; Ankner, J. F.; Douglas, J. F.; Karim, A. Hiking down the Free Energy Landscape Using Sequential Solvent and Thermal Processing for Versatile Ordering of Block Copolymer Films. *ACS Appl. Mater. Interfaces* **2023**, *15* (17), 21562−21574.
(12) Modi, A.; Bhaway, S. M.; Vogt, B. D.; Douglas, J. F.; Al-Enizi, A.; Elzatahry, A.; Sharma, A.; Karim, A. Direct Immersion Annealing of Thin Block Copolymer Films. *ACS Appl. Mater. Interfaces* **2015**, *7* (39), 21639−21645.
(13) Longanecker, M.; Modi, A.; Dobrynin, A.; Kim, S.; Yuan, G.; Jones, R.; Satija, S.; Bang, J.; Karim, A. Reduced Domain Size and Interfacial Width in Fast Ordering Nanofilled Block Copolymer Films by Direct Immersion Annealing. *Macromolecules* **2016**, *49* (22), 8563−8571.
(14) Zhang, X.; Harris, K. D.; Wu, N. L. Y.; Murphy, J. N.; Buriak, J. M. Fast Assembly of Ordered Block Copolymer Nanostructures through Microwave Annealing. *ACS Nano* **2010**, *4* (11), 7021−7029.
(15) Gotrik, K. W.; Ross, C. A. Solvothermal Annealing of Block Copolymer Thin Films. *Nano Lett.* **2013**, *13* (11), 5117−5122.
(16) Majewski, P. W.; Yager, K. G. Millisecond Ordering of Block Copolymer Films via Photothermal Gradients. *ACS Nano* **2015**, *9* (4), 3896−3906.
(17) Majewski, P. W.; Gopinadhan, M.; Osuji, C. O. Magnetic Field Alignment of Block Copolymers and Polymer Nanocomposites: Scalable Microstructure Control in Functional Soft Materials. *J. Polym. Sci. B Polym. Phys.* **2012**, *50* (1), 2−8.
(18) Xu, T.; Zvelindovsky, A. V.; Sevink, G. J. A.; Lyakhova, K. S.; Jinnai, H.; Russell, T. P. Electric Field Alignment of Asymmetric Diblock Copolymer Thin Films. *Macromolecules* **2005**, *38* (26), 10788−10798.
(19) Zeman, L.; Patterson, D. Effect of Solvent on Polymer Incompatibility in Solution. *Macromolecules* **1972**, *5* (4), 513−516.
(20) Cummins, C.; Mokarian-Tabari, P.; Andreazza, P.; Sinturel, C.; Morris, M. A. Solvothermal Vapor Annealing of Lamellar Poly-(Styrene)-Block-Poly(d,l-Lactide) Block Copolymer Thin Films for Directed Self-Assembly Application. *ACS Appl. Mater. Interfaces* **2016**, *8* (12), 8295−8304.
(21) Shi, L. Y.; Lan, J.; Lee, S.; Cheng, L. C.; Yager, K. G.; Ross, C. A. Vertical Lamellae Formed by Two-Step Annealing of a Rod-Coil Liquid Crystalline Block Copolymer Thin Film. *ACS Nano* **2020**, *14* (4), 4289−4297.
(22) Tanaka, H.; Tomita, H.; Takasu, A.; Hayashi, T.; Nishi, T. Morphological and Kinetic Evolution of Surface Patterns in Gels during the Swelling Process: Evidence of Dynamic Pattern Ordering. *Phys. Rev. Lett.* **1992**, *68* (18), 2794−2797.
(23) Stafford, C. M.; Harrison, C.; Beers, K. L.; Karim, A.; Amis, E. J.; Vanlandingham, M. R.; Kim, H. C.; Volksen, W.; Miller, R. D.; Simonyi, E. E. A Buckling-Based Metrology for Measuring the Elastic Moduli of Polymeric Thin Films. *Nat. Mater.* **2004**, *3* (8), 545−550.
(24) Chung, J. Y.; Nolte, A. J.; Stafford, C. M. Surface Wrinkling: A Versatile Platform for Measuring Thin-Film Properties. *Adv. Mater.* **2011**, *23* (3), 349−368.
(25) Coulon, G.; Russell, T. P.; Deline, V. R.; Green, P. F. Surface-Induced Orientation of Symmetric, Diblock Copolymers: A Secondary Ion Mass Spectrometry Study. *Macromolecules* **1989**, *22* (6), 2581−2589.
(26) Russell, T. P.; Coulon, G.; Deline, V. R.; Miller, D. C. Characteristics of the Surface-Induced Orientation for Symmetric Diblock PS/PMMA Copolymers. *Macromolecules* **1989**, *22* (12), 4600−4606.
(27) Anastasiadis, S. H.; Russell, T. P.; Satija, S. K.; Majkrzak, C. F. Neutron Reflectivity Studies of the Surface-Induced Ordering of Diblock Copolymer Films. *Phys. Rev. Lett.* **1989**, *62* (16), 1852−1855.
(28) Park, S.; Wang, J. Y.; Kim, B.; Chen, W.; Russell, T. P. Solvent-Induced Transition from Micelles in Solution to Cylindrical Microdomains in Diblock Copolymer Thin Films. *Macromolecules* **2007**, *40* (25), 9059−9063.
(29) Peng, J.; Xuan, Y.; Wang, H.; Yang, Y.; Li, B.; Han, Y. Solvent-Induced Microphase Separation in Diblock Copolymer Thin Films with Reversibly Switchable Morphology. *J. Chem. Phys.* **2004**, *120* (23), 11163−11170.
(30) Masud, A.; Longanecker, M.; Bhadauriya, S.; Singh, M.; Wu, W.; Sharma, K.; Terlier, T.; Al-Enizi, A. M.; Satija, S.; Douglas, J. F.; Karim, A. Ionic Liquid Enhanced Parallel Lamellar Ordering in Block Copolymer Films. *Macromolecules* **2021**, *54* (10), 4531−4545.
(31) Smith, A. P.; Douglas, J. F.; Amis, E. J.; Karim, A. Effect of Temperature on the Morphology and Kinetics of Surface Pattern Formation in Thin Block Copolymer Films. *Langmuir* **2007**, *23* (24), 12380−12387.
(32) Smith, A. P.; Douglas, J. F.; Meredith, J. C.; Amis, E. J.; Karim, A. Combinatorial Study of Surface Pattern Formation in Thin Block Copolymer Films. *Phys. Rev. Lett.* **2001**, *87*, 1.
(33) Stasiak, P.; McGraw, J. D.; Dalnoki-Veress, K.; Matsen, M. W. Step Edges in Thin Films of Lamellar-Forming Diblock Copolymer. *Macromolecules* **2012**, *45* (23), 9531−9538.
(34) Maher, M. J.; Self, J. L.; Stasiak, P.; Blachut, G.; Ellison, C. J.; Matsen, M. W.; Bates, C. M.; Willson, C. G. Structure, Stability, and Reorganization of 0.5 L0 Topography in Block Copolymer Thin Films. *ACS Nano* **2016**, *10* (11), 10152−10160.
(35) Ahn, H.; Ryu, D. Y.; Kim, Y.; Kwon, K. W.; Lee, J.; Cho, J. Phase Behavior of Polystyrene-b-Poly(Methyl Methacrylate) Diblock Copolymer. *Macromolecules* **2009**, *42* (20), 7897−7902.
(36) Vandeparre, H.; Damman, P. Wrinkling of Stimuloresponsive Surfaces: Mechanical Instability Coupled to Diffusion. *Phys. Rev. Lett.* **2008**, *101* (12), No. 124301, DOI: 10.1103/PhysRevLett.101.124301.
(37) Li, B.; Cao, Y. P.; Feng, X. Q.; Gao, H. Mechanics of Morphological Instabilities and Surface Wrinkling in Soft Materials: A Review. *Soft Matter.* **2012**, *7*, 5728−5745.
(38) Kang, M. K.; Huang, R. Effect of Surface Tension on Swell-Induced Surface Instability of Substrate-Confined Hydrogel Layers. *Soft Matter* **2010**, *6* (22), 5736−5742.
(39) Gránásy, L.; Pusztai, T.; Douglas, J. F. Insights into Polymer Crystallization from Phase-Field Theory. In *Encyclopedia of Polymers and Composites*; Springer: Berlin Heidelberg, 2013; pp 1−35.
(40) Koneripalli, N.; Bates, F. S.; Fredrickson, G. H. Fractal Hole Growth in Strained Block Copolymer Films. *Phys. Rev. Lett.* **1998**, *81* (9), 1861−1864.
(41) Chung, J. Y.; Nolte, A. J.; Stafford, C. M. Diffusion-Controlled, Self-Organized Growth of Symmetric Wrinkling Patterns. *Adv. Mater.* **2009**, *21* (13), 1358−1362.
(42) Ferreiro, V.; Douglas, J. F.; Warren, J.; Karim, A. Growth Pulsations in Symmetric Dendritic Crystallization in Thin Polymer Blend Films. *Phys. Rev. E Stat Phys. Plasmas Fluids Relat Interdiscip Topics* **2002**, *65* (5), 16.
(43) Beers, K. L.; Douglas, J. F.; Amis, E. J.; Karim, A. Combinatorial Measurements of Crystallization Growth Rate and Morphology in Thin Films of Isotactic Polystyrene. *Langmuir* **2003**, *19* (9), 3935−3940.
(44) Douglas, J. F.; Efimenko, K.; Fischer, D. A.; Phelan, F. R.; Genzer, J. Propagating Waves of Self-Assembly in Organosilane

Monolayers. *Proc. Natl. Acad. Sci. U.S.A.* **2007**, *104* (25), 10324−10329.
(45) Smith, A. P.; Douglas, J. F.; Amis, E. J.; Karim, A. Effect of Temperature on the Morphology and Kinetics of Surface Pattern Formation in Thin Block Copolymer Films. *Langmuir* **2007**, *23* (24), 12380−12387.
(46) Smith, A. P.; Douglas, J. F.; Meredith, J. C.; Amis, E. J.; Karim, A. High-Throughput Characterization of Pattern Formation in Symmetric Diblock Copolymer Films. *J. Polym. Sci. Part B: Polym. Phys.* **2001**, *39*, 2141−2158.
(47) Kim, S.; Bates, C. M.; Thio, A.; Cushen, J. D.; Ellison, C. J.; Willson, C. G.; Bates, F. S. Consequences of Surface Neutralization in Diblock Copolymer Thin Films. *ACS Nano* **2013**, *7* (11), 9905−9919.
(48) Modi, A.; Karim, A.; Tsige, M. Solvent and Substrate Induced Synergistic Ordering in Block Copolymer Thin Films. *Macromolecules* **2018**, *51* (18), 7186−7196.
(49) Anastasiadis, S. H.; Russell, T. P.; Satija, S. K.; Majkrzak, C. F. The Morphology of Symmetric Diblock Copolymers as Revealed by Neutron Reflectivity. *J. Chem. Phys.* **1990**, *92* (9), 5677−5691.
(50) Cabral, J. T.; Hudson, S. D.; Harrison, C.; Douglas, J. F. Frontal Photopolymerization for Microfluidic Applications. *Langmuir* **2004**, *20* (23), 10020−10029.
(51) Cabral, J. T.; Douglas, J. F. Propagating Waves of Network Formation Induced by Light. *Polymer (Guildf)* **2005**, *46* (12), 4230−4241.
(52) Milner, S. T.; McLeish, T. C. B. Parameter-Free Theory for Stress Relaxation in Star Polymer Melts. *Macromolecules* **1997**, *30* (7), 2159−2166.
(53) Milner, S. T.; McLeish, T. C. B.; Young, R. N.; Hakiki, A.; Johnson, J. M. Dynamic Dilution, Constraint-Release, and Star - Linear Blends. *Macromolecules* **1998**, *31* (26), 9345−9353.
(54) Milner, S. T.; Mc Leish, T. C. B. Reptation and Contour-Length Fluctuations in Melts of Linear Polymers. *Phys. Rev. Lett.* **1998**, *81* (3), 725−728.
(55) Milner, S. T.; McLeish, T. C. B. Arm-Length Dependence of Stress Relaxation in Star Polymer Melts. *Macromolecules* **1998**, *31* (21), 7479−7482.
(56) Douglas, J. F.; Hubbard, J. B. Semiempirical Theory of Relaxation: Concentrated Polymer Solution Dynamics. *Macromolecules* **1991**, *24*, 3163−3177.
(57) Mortezaei, M.; Famili, M. H. N.; Kokabi, M. The Role of Interfacial Interactions on the Glass-Transition and Viscoelastic Properties of Silica/Polystyrene Nanocomposite. *Compos. Sci. Technol.* **2011**, *71* (8), 1039−1045.
(58) Wu, S. Calculation of Interfacial Tension in Polymer Systems. *J. Polymer. Sci.: Part C* **1971**, *34*, 19−30.
(59) Turner, M. S. Equilibrium Properties of a Diblock Copolymer Lamellar Phase Confined between Flat Plates. *Phys. Rev. Lett.* **1992**, *69* (12), 1788.
(60) Walton, D. G.; Kellogg, G. J.; Mayes, A. M.; Lambooy, P.; Russell, T. P. A Free Energy Model for Confined Diblock Copolymers. *Macromolecules* **1994**, *27* (21), 6225−6228.

https://doi.org/10.1021/acsami.4c00068
ACS Appl. Mater. Interfaces 2024, 16, 15569−15585